A Biologically-Inspired Model for a Spiking Retina

Adrien Wohrer, Pierre Kornprobst, Thierry Viéville

INSTITUT NATIONAL DE RECHERCHE EN INFORMATIQUE ET EN AUTOMATIQUE

A Biologically-Inspired Model for a Spiking Retina

Adrien Wohrer — Pierre Kornprobst — Thierry Viéville

N° 5848

Février 2006

Thème BIO

ISSN 0249-6399

A Biologically-Inspired Model for a Spiking Retina

Adrien Wohrer* , Pierre Kornprobst† , Thierry Viéville‡

Thème BIO — Systèmes biologiques
Projet Odyssée

Rapport de recherche n° 5848 — Février 2006 — 78 pages

Abstract: The purpose of this research is to provide potential neuroscientists and computer scientists with an artificial retina model, delivering spikes to higher-level visual tasks simulations. The architecture of our retina model is based on recent physiological studies, so that each feature is related to real retina characteristics. The model includes a linear filtering process, followed by a static non-linearity, and then a spike generation process. It thus simulates the output of the Parvocellular pathway of primate retinas, possibly for large-scale simulations. Two series of tests were performed: firstly on single cells for which ground truth is available, secondly on realistic visual scenes. The report sets the basis for further modeling. This includes nonlinear effects that could occur due to the conductance-based nature of synaptic interactions. Another future extension is modeling of the Magnocellular pathway of primate retinas. It is our conviction that building such a bio-inspired model will help in better understanding how the retina performs and also in relating observations to biological mechanisms.

Key-words: Retina, Visual system, Spikes, Physiology, Simulator, Retinotopy, Conductances.

* Adrien.Wohrer@sophia.inria.fr
† Pierre.Kornprobst@sophia.inria.fr
‡ Thierry.Vieville@sophia.inria.fr

Un modèle de Rétine à Spikes d'Inspiration Biologique

Résumé : Ce rapport a pour but la création d'un modèle de rétine artificielle, capable de convertir l'information visuelle en séries d'émissions de potentiels d'action. Ce modèle se veut un outil de simulation pour les neuroscientifiques, mais également une possible entrée pour des systémes de vision artificielle basés sur du codage par temps discrets. Le modèle puise son inspiration directement dans la physiologie, et chacune de ses composantes peut être rattachée à une localisation physiologique précise. Ces composantes sont au nombre de trois: un filtrage spatio-temporal, suivi d'une non-linéarité statique puis d'un processus d'émission de spikes. Le modèle résultant simule le fonctionnement de la voie Parvocellulaire des rétines des primates. Pour tester le modèle, nous simulons le comportement d'une seule cellule et le comparons à des enregistements physiologiques, puis nous simulons la réponse d'une rétine entière à des stimulations visuelles. Nous proposons un cadre théorique pour les neurones de notre modèle, qui permettra d'étudier les potentiels effets non-linéaires dus à la nature des courants ioniques dans les neurones, qui sont véhiculés par des ouvertures de conductances. Nous proposons également des pistes pour étendre le modèle à la voie Magnocellulaire de la rétine du primate. Nous sommes persuadés qu'un modèle attaché autant que possible à la physiologie permettra de mieux relier les observations expérimentales à l'architecture biologique qui leur donne naissance.

Mots-clés : Rétine, Système visuel, Spikes, Physiologie, Simulateur, Rétinotopie, Conductances.

Contents

1 The Retina: a Powerful Machinery

The visual system and the associated eye-control motor system take a significant percentage (a few tens of percents) of the whole cortex in the human brain. In this scope, the input to all these systems, i.e. the retina, is likely to carry out a lot of information. A human retina (Figure 1) concentrates about 10^8 photoreceptors within a diameter of about 4cm [36] and the transmission rate of the retina is estimated between 10^5 and 10^6 bits per second.

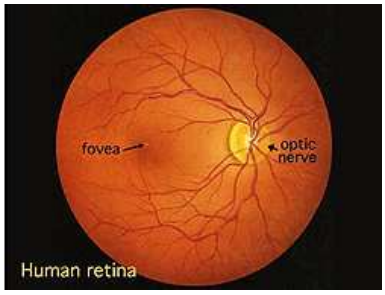

Figure 1: Human retina seen through an ophtalmoscope (from [26])

The retina is strongly structured. Not only is it organized in layers, with five generic types of cells, but also different *pathways* co-exist inside these layers. These pathways correspond to information streams dealing with different spatial and temporal scales of the visual flux. Furthermore, in the case of primates or mammalians with frontal vision, the retina possesses a radial organization: its center, known as the *fovea* in primates, is subject to very detailed (and thus, energy demanding) processing, such as reading.

The cells in the retina can be considered as neurons, due to their electrical properties and their connectivity. However, as opposed to cortical neurons, most retinal cells do not fire any *action potentials*, or *spikes*. Only the cells in the last layer (called ganglionar cells) fire and send the encoded visual information to the brain via the optical nerve.

The incredible complexity of our environment (traditionally referred to as "natural scenes") requires particular performances from the retina. The unbounded quantity of information has to be compressed through our visual system, which has a finite information capacity. And, despite this is mainly provided by the LGN and cortical structures, such processing comes out though the biggest step in information compression: the retina. As a finite capacity channel from the environment (the natural scenes), the retina sets the quantity of information to be processed by the whole visual system.

From the point of view of information theory, the retina sets the processing capacity of the whole visual system. As a finite capacity channel from an environment with infinite information (the natural scenes), the retina necessarily performs compression of the visual information and, for the visual system to be efficient, this compression must be adapted to the external environment. The retina compresses information at three levels. First, a low-pass filtering of the visual input is provided by the receptors, since they integrate (spatially and temporally) and *sample* (spatially, as a digital camera) the light projected onto the back of the eye. Then comes another challenge the retina has to deal with: the average luminance of a natural scene varies drastically according to location, daytime, etc. In fact, a single receptor can receive as few as one photon every ten minutes, under star light, and as much as 10^5 photons per second under bright sunlight. The luminance range thus varies in a factor of 10^8 at least! We animals do not need much information about luminance,

but rather about the objects reflecting the light. As a consequence, our retina provides a large invariance with respect to luminance: retinal output has similar orders of magnitude in all luminance conditions. This invariance is mostly provided by the light receptors in the retina, although additional adaptation to luminosity is also provided by the next layers of the retina. Finally, at a third level, information in the retina is compressed in a way that stresses the underlying *causes* of our visual stimulation: what we call objects. Statistically and geometrically, most objects create *edges* on the retina, that is large and local variations of the light intensity. Thanks to the specific connectivity of retinal layers, the biggest amount of information processed by the retina is located on object edges.

Section 2 presents the anatomical properties of the retina. Section 3 details our modeling framework for retinal neurons and their interactions. Section 4 presents our model for the output of ganglionar cells from the *Parvocellular* pathway, and the way we have implemented it. The luminance invariance, edge detection, and compression mechanisms, will appear naturally in this model. Furthermore, the foveated structure will be taken into account. Section 5 present simulations and validations of this model, for single cells and a simulated retina, with several visual stimuli. A discussion on the present model is provided in Section 6, and possible developments are exposed in Section 7, including modeling of the *Magnocellular* pathway of the retina.

2 Anatomy and Functionality of the Retina

2.1 Filtering Structure

2.1.1 Overview

The goal of this section is to describe the retinal mechanism as a filtering structure, and to provide an overview of the links between anatomy and the related functional behavior. As a result, we propose in Figure 2 a schematic view of the retina, which will be used in the rest of the paper. This section shows how it is related to anatomical facts.

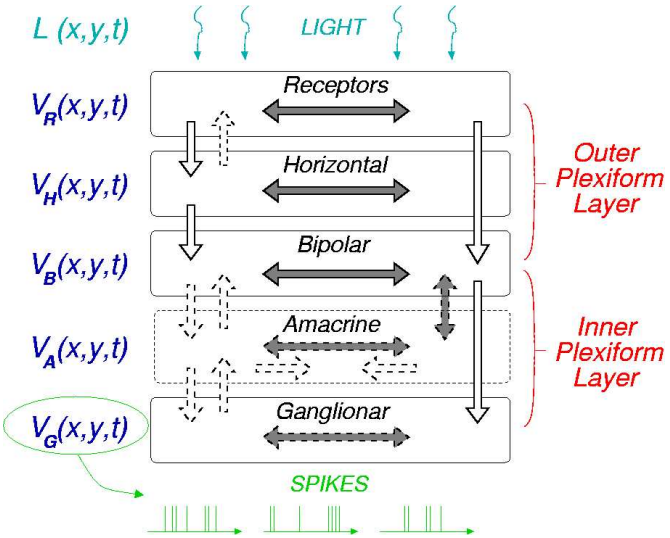

Figure 2: Schematic view of the filtering occurring in the retina. Layers of cells are represented by boxes connected through synaptic interactions. $V_R(x, y, t)$, etc. represent the potentials of the cells in each layer at time t, with (x, y) being the spatial coordinates of the considered cell. Two distinct synaptic layers, the OPL and the IPL, define two successive filtering stages. $V_G(x, y, t)$ defines the membrane potentials of all ganglionar cells. It contains the information sent to the brain by the retina, consisting of one spike train per ganglionar cell.

2.1.2 Organization in Connected Layers

The retina contains five different types of visual cells. Figure 3(a) shows a section of a real mammalian retina and its anatomical interpretation. Cells of the same type form a *layer*, paving the whole retina. Layers are connected as described in Figure 3(b), and summarized

in Figure 2. Retinal cells are *neurons*, that encode signal through their electrical membrane potential. We will consider them as *point neurons*, meaning that the potential of a cell at time t is defined by a unique number $V(t)$.

We can then append the activities for all the cells within a layer. If cell density is dense enough, the activities of all the cells in the layer define a spatially continuous function representing the activity of the layer at time t. For example, $(x, y) \rightarrow V_B(x, y, t)$ represents the activities of bipolar cells at time t (see Figure 2). The retina can be seen as a filtering scheme that transforms its light input into trains of spikes thanks to five successive layers, each layer being described by a population function.

Interactions can occur between cells from different layers, and also between cells of the same layer. But the nature of these interactions are different:

Chemical synapses

Chemical synapses link cells from different layers. All chemical synapses occur in two *plexiform* layers (Figure 3(a)): the Outer Plexiform Layer (OPL) and the Inner Plexiform Layer (IPL). These two layers of synapses define *two (almost) independent processing stages*, as represented in Figure 2. Section 3.2 presents our model for a chemical synapse in the retina.

Electrical synapses, also called gap junctions

This kind of synapses link neighboring cells *of the same layer*, allowing some intra-layer communication[1]. Such junctions are present with different strengths in each of the five layers, and result in a local sharing of the information between cells of the same type. Section 3.3 provides a simple approximation for this sharing of information.

2.1.3 Five Types of Cells

In this Section, we briefly describe the five layers of the retina. We will come back to them when modeling the retina (Section 4).

Receptors

Receptors receive, sample and integrate the light arriving at the back of the eye. They are of two kinds: *cones* and *rods* (both represented on top of Figure 3 (b)). Cones are activated at high illumination levels (daytime). They are the most useful source of information for precise shape analysis. There are three types of cones, sensitive to different wavelengths (Red, Green and Blue): cones encode color. Figure 4 shows a paving by cones in a primate eye[2].

[1] Note that some gap junctions also exist between different cell types, for example between the amacrine cell AII and cone bipolar cells [25, 26].

[2] Short wavelength, or 'Blue' cones, are much sparser than the other two. They are actually the oldest 'color cones'. Most mammals possess a basic bi-chromatic vision, with a dominant 'middle wavelength' type of cone, and a sparser 'blue' cone, specialized in color information. Only in primates has the 'middle cone'

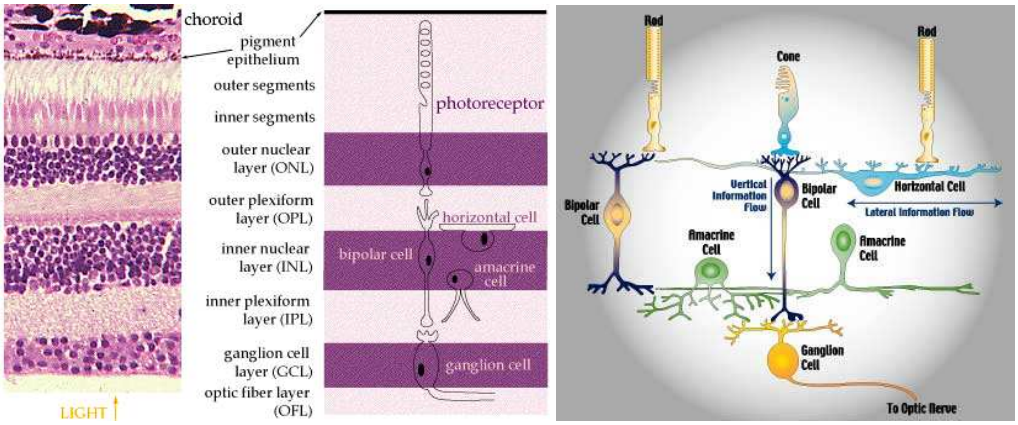

(a) Vertical section of a retina (b) Five retinal cell types

Figure 3: (a) Vertical section of a retina. There are five cell types, whose nuclei are located in three layers, and that make their connections in two plexiform layers. From [32]. (b) Schematic view of the five cell types and their connections. Found at [8].

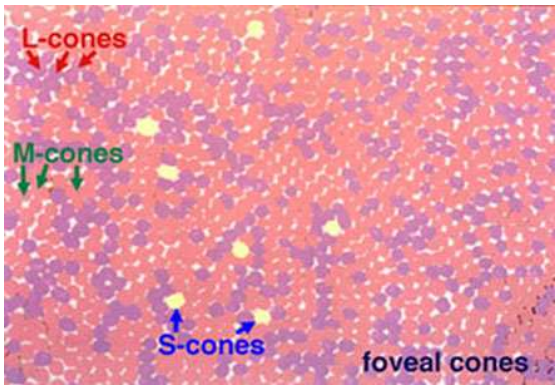

Figure 4: Paving of a primate fovea by cones. Notice how sparse short wavelength ('Blue') cones are. From [26], reproduced from *Lall and Cone, 1996.*

On the contrary, rods exist in a single version: they only see "in black and white". Rods are very sensitive to luminosity, and their response saturates at high illumination (daytime). They are much more numerous than cones, except at the very center of the eye (the fovea). The rod signal is most useful at night, or for movement detection. Phylogenetically, rods seem to have appeared later in the evolution.

The integration of light by receptors is known as *phototransduction* (see Section 4.1.1). The output signal of the receptors is then transmitted to horizontal cells and bipolar cells, in the OPL.

Horizontal cells

Horizontal cells relay the signal from the receptors (through chemical synapses in the OPL), and are also highly coupled to their neighboring horizontal cells (through electrical synapses). This coupling makes them sensitive to a more spatially *blurred*, or low-passed, version of the image than the receptors (see Section 4.2). Furthermore, since their membrane *integrates* the input from the receptors, they also *temporally* low-pass the signal from receptors. They make feedback connections to receptors, and also feed-forward connections to bipolar cells.

Bipolar cells

Still at the level of the OPL, bipolar cells are connected with both receptors and horizontal cells. But the sign of these two types of connexions are always different: if a bipolar cell is depolarized by the signal of receptors, it is hyperpolarized by the signal of horizontal cells, and vice-versa. Hence, a bipolar cell is always sensitive to a difference between the signal from receptors and its blurred version by the horizontal cells.

Such excitatory/inhibitory interactions are very classical in neural networks and are known as *synaptic triads*. The synaptic triad makes bipolar cells spatial and temporal *band-pass* filters: they behave like edge detectors. According to the respective signs of the connexions from receptors and horizontal cells, there will be ON-center cells and OFF-center cells (Section 4.3).

Bipolar cells are also the input to the second filtering stage of the retina, the IPL. They possess an elongated structure with two dendritic trees (Figure 3 (b)), that gave them their name of 'bipolar'.

Amacrine cells

Synaptic exchanges in the IPL are relatively similar to those in the OPL, but less well understood. Indeed, amacrine cells, that play the same interstitial role as horizontal cells in the OPL, are a very *diverse* class of cells. Amacrine cells have different sizes, physiology and functions that are not all well understood. We do not explicitly model them, but report some of their supposed functions in Section 4.4.2.

divided in two equally-present versions, the 'Red' and the 'Green' cone, that make the whole cone pathway chromatic, with three channels. See [31].

Ganglionar cells

Ganglionar cells receive signal from bipolar and amacrine cells. They are the output of the retina, and they all fire *spikes* to the brain. They are the only spiking cells of the retina, along with some amacrine cells. Their spike generation process is modeled in Section 4.4.1.

2.1.4 Linearity of the Two Filtering Stages?

The two plexiform layers perform almost independent filtering stages (Figure 2). Are these filtering stages linear? i.e. does the output of a ganglionar cell depend linearly on the incoming light? The answer is no for two reasons. First reason is that light receptors do not react linearly at all to the incoming light intensity, otherwise our retina would be 10^5 times more active in bright daylight than in room light (see Section 4.1). Second reason is that retinal cells are linked through synapses, that perform non linear operations.

However, a linear approximation has physiological validation when the general light intensity is at a fixed level (to insure some linearity in the conversion from light intensity to receptor activity), and for a particular pathway of ganglionar cells. Section 2.2 presents the two main *pathways* of information flowing out of the retina: one of them (the Parvocellular pathway) is grossly linear, whereas the other (the Magnocellular pathway) is not. But whatever the pathway considered, most retinal models use linear filters at some point, because they are much better understood, and easier to implement. In Section 3, we define a framework to model neurons that allows the retina to work linearly in a certain range of parameters.

The linear approximation for ganglionar has long been proposed [41], inspired by previous study on ganglionar receptive fields [23]. The *receptive field* (RF) of the cell is defined by the area of the visual field where a light stimulation has an influence on the firing of the cell, when the rest of the visual field is not stimulated (gray field)[3]. Figure 7 gives an idea of the sizes of the receptive fields in the retina.

Given a cell centered in x_0 on the retina, and with receptive field RF, a linear approximation of its activity consists in finding the kernel K for which the following equation is best verified:

$$\mathrm{A}(x_0) = \int_{\mathrm{RF}(x_0)} I(x_0 + x)\, K(x)\, \mathrm{d}x,$$

where I is the luminosity profile of the image, and A is a measure of activity appropriate to the type of cell (its membrane potential if it is a non-spiking cell, or its instantaneous firing-rate if it is a spiking cell). By extent, K is often described as the *linear receptive field* of the cell. As remarked by [41], K can be correctly approximated by a *Difference of Gaussians* (DOG). Depending on the global sign of K, the cell is called an ON-center cell

[3]Note that the **receptive field** of a visual cell is a word that conveys various meanings. The *non-classical* receptive field describes the visual region that has *potential* influence on the firing of the cell, although a light stimulation in this region does not modify the firing if the rest of the scene is a gray field. It is a secondary influence, requiring stimulation on the classical receptive field.

(with OFF surround), or an OFF-center cell (with ON surround). In Section 4 we will find this structure of the receptive field to appear very naturally at the level of the OPL.

2.2 Different Pathways

As we have just said, only a portion of ganglionar cells have answers well approximated by linear summation. Indeed, differences in anatomy and physiology define two main types of ganglionar cells [15]. These two types are actually the output of two different retinal **pathways**, that do not imply the same cells. Physiologically, this means that the basic 5-layers architecture presented above is parallelized in multiple versions, physically imbricated but with little interactions from one pathway to another[4]. We refer to [31, 26] for a more precise view.

Functionally, correspondence exists between the two retinal pathways and the two pathways of information in the brain: *Form* pathway and *Motion* pathway. In the brain, a ventral route ('Form') is dedicated to precisely studying the shapes of objects (face recognition, texture recognition, etc.), while a dorsal route ('Movement'), involving different areas, is specialized in movement analysis (movements of objects, self-motion of the observer, etc.) Although there is no trivial correspondence, the retinal Parvocellular pathway naturally provides a good input to the brain's Form pathway, and the retinal Magnocellular pathway provides naturally a good input for the brain's Motion pathway, for reasons that we explain now.

Parvocellular pathway (P)

The Parvocellular pathway consists of ganglionar cells with small receptive fields and persistent reaction to intensity changes, whose generic name across species is **β cells**. They are known as *Midget* cells in the primate retina, and as X cells in the cat retina. As can be seen in Figure 5(A), they are well modeled by a linear receptive field. They have a significant *steady firing rate* (without visual stimulation), that allows them to code signals both by increase or decrease of their firing. They exist in both ON and OFF versions.

There are differences in β cells according to the species considered. Primate Midget cells have smaller receptive fields than cat X cells, that allow very accurate spatial resolution. Also, most cat X Cells see in black and white, whereas all Midget cells are color opponents: their receptive field structure consists of a central excitation zone sensitive to one color (e.g. Red), and a peripheral inhibition zone sensitive to another (e.g. Green). There are roughly two different color opposition signals in primate retinas: Red/Green and Yellow/Blue. Notice that this property requires that Midget cells take their input mainly from cones. Finally, Midget cells are much more numerous in primate retina than X Cells are in cat retina.

Whatever the species considered, spatial precision and color sensitivity make β cells a good input to the 'Form' pathway of the brain. And indeed, their persistent answer to illumination changes requires the scene not to move too fast: these cells are mostly designed

[4]This is however a very schematic view. Interactions exist between many cell types, as a glance at web site [26] clearly demonstrates.

for fixating objects, which also explains their huge number in primate and humans, animals involved in precise visual tasks. β-cells are the ganglionar cells modeled in this report.

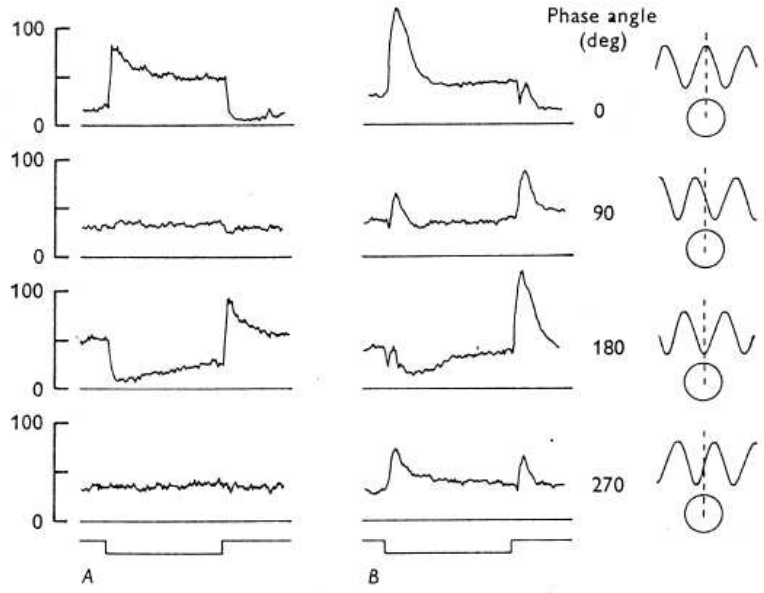

Figure 5: Trial-averaged firing rates of a cat OFF-center X cell, and of an OFF-center Y cell, in response to the introduction and removal of a static image, displaying a sinusoidal grating with different spatial offsets (right). If the cell can indeed be modeled by a linear kernel, then there will be an offset of the grating for which its answer is the same as without any stimulus, when the positive and negative parts of its signal counterbalance each other. X cells verify this property, whereas Y cells don't, meaning that there is some spatial non-linearity in their processing. Note also that Y cells are more transient than X cells (short peak of answer). Total experience time 2s. From [15].

Magnocellular pathway (M)

The Magnocellular pathway consists of large cells, whose generic name across species is **α cells**. They correspond to the primate's *Parasol* cells, and to the cat's *Y* cells. They have a much wider receptive field than β cells, are only sensitive to rapid intensity changes, and transmit spikes very rapidly to the brain. They also exist in both ON and OFF versions.

α cells are not sensitive to color opposition, but only to luminosity (black and white), because they take their input from rods[5], and indistinctly from all three types of cones. The wide receptive field, meaning little spatial precision, and the fast transmission, meaning temporal reliability, make these cells a good input for the 'Movement' pathway of the brain.

Physiologically, α cells are temporally *transient*, meaning that they only react to intensity changes in time, remaining mostly quiet otherwise. Furthermore, they do not sum their spatial input linearly. A typical proof of their non-linearity is that even harmonics appear in their answer to a drifting grating, which implies a *rectification* of the signal at some point in the Magnocellular pathway [21]. Another proof of their spatial non-linearity is given in Figure 5. This non-linearity makes α cells harder to model. In this report we only propose physiological findings, as cues for future modeling.

Remark Many other types of ganglionar cells exist, whose characteristics are less well-known than α and β cells. They include the so-called *koniocellular* cells, whose functional role remains unclear, some *directional selective* cells [2], and even very wide-field cells involved in general luminosity appreciation or circadian rhythms [31]. Many of these other cell types, common in other mammals such as rabbits, were long thought absent of primate retinas. It now appears more likely that primates also possess them, but drowned in a greater number of β and α cells, that statistically "hides" them [31].

2.3 Radial Organization

When one wants to have a precise look at an object, one needs to move the eyes on it, so as to have the considered object projected at the very center of the retina. This is because, in some species including primates, the retina exhibits a particular radial structure. The central region of the retina is known as the *fovea*. In humans, it covers about 6 degrees of visual field, the size of a fist at length of arm. Humans even possess an more precise zone in the very center of the retina (diameter of 1.5 degrees, one or two fingers at length of arm) called the *foveola*, at the core of our ability to execute very precise visual tasks such as reading.

Figure 6 shows the densities of both types of receptors in a human retina, as a function of eccentricity r (distance from the center of retina). The density of cones follows a typical power law, proportional to r^{-1}. This translates into our decreasing ability to precisely see objects far from the center of our retina. On the contrary, the density of rods reaches its peak at around 20 degrees of eccentricity. Then it decreases slowly, but no power law exists as obviously as for cones. Rods are much more numerous than cones, especially in peripheral regions. The great number of rods allows the retina to detect subtle illumination changes through *population coding*, even in the daytime when they are mostly saturated. It makes rod signal a good basis for movement detection. The counterpart of their population coding

[5] rods do not possess specific ganglion cells, but rather transmit their signal to the cone pathway at the level of AII amacrine cells [25].

is the loss of spatial acuity. For this reason, the fovea doesn't contain rods: it is dedicated to precise, daytime, shape analysis based on cone signals.

The density decrease is not only observed for receptors, but also for all retinal cell types, including ganglionar cells, although the power law with r might not be exactly the same. In the same time, the size of their dendritic tree increases, meaning *increasing receptive fields*. This second fact appears very natural from the point of view of sampling. If each retinal cell is seen as sampling a continuous signal at some point of the retina, a decrease in the density of one type of cell means a decrease of the sampling frequency of the corresponding continuous signal. To avoid aliasing, the signal must be more low-passed when the sampling frequency gets smaller, which the cells insure by increasing the size of their receptive fields. The perceptual consequence is that the image becomes way less precise far from the fovea.

Figure 7 is a recording of the sizes of ganglionar cell dendritic trees, that provide a good estimate of their receptive field sizes. It illustrates the general increase of receptive fields with eccentricity r. The authors [9] estimate the average Midget dendritic tree to approximately scale with r, while Parasol cells rather scale with $r^{0.65}$.

These power laws are interesting to compare with the receptor densities illustrated in Figure 6, and in particular with cone density that grossly scales with r^{-1}. Midget cells receive their inputs mostly from cones, and their dendritic trees follow a law inversely proportional to cone density: this suggests that the whole cone pathway might scale with r. Conversely, Parasol cells receive a mixed input of rods and cones, and rod density decreases much slower than cone density. As a result, the Parasol receptive field size increases *slower* with eccentricity, with a power law approximated by $r^{0.65}$.

Figure 7 also shows the discrepancy in receptive field sizes between Midget and Parasol cells, whose receptive fields at the same eccentricity are five to ten times wider. Finally, we see a good estimation for the internal variation of scale inside the same pathway. At a given eccentricity, receptive fields sizes vary within one or two octaves only.

After this physiological presentation of the retina, but before going deeper into our model, we present the mathematical framework we have used to understand interactions between cells.

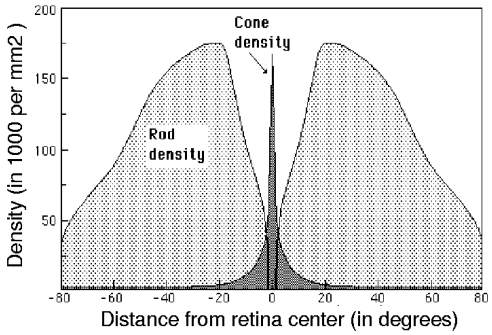

Figure 6: Density of receptors found in human retina. Reproduced from [36].

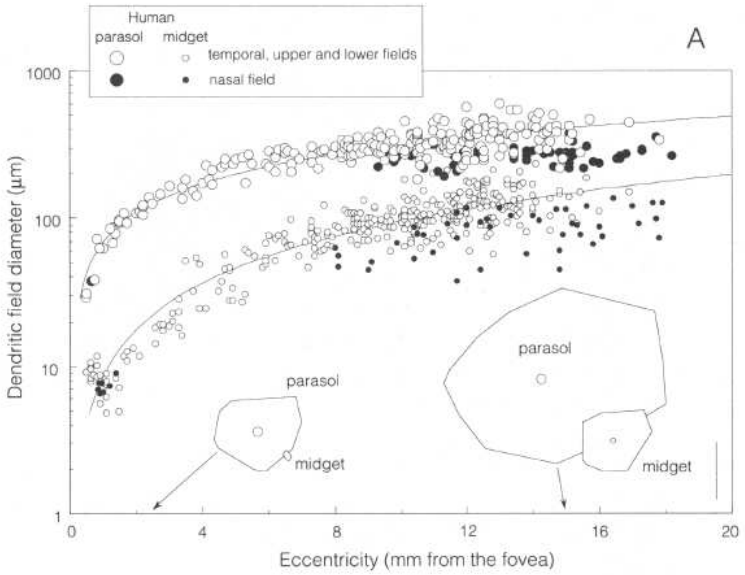

Figure 7: Measurements of ganglionar dendritic tree sizes with respect to eccentricity. From [9].

3 Neuron Modeling in the Retina

In this section we present our model for retinal neurons and their synaptic interactions. Our basic assumption is that retinal cells can be modeled as *point neurons*, which means that we neglect the spatial structure of the neurons[6]. The membrane potentials of the neurons are denoted by $V(t)$.

3.1 Internal Model for a Neuron

We present here our model for the internal equation that drives a neuron's potential as a function of its inputs. We chose the framework of conductance-driven neurons. This choice allows to stick closer to the biological nature of ionic currents in neurons, and it is our conviction that specific non-linear effects can be explained by using such a conductance-based framework rather than simple current-driven neurons.

3.1.1 The Integration Equation

Channel model. A neuron has ionic channels in its membrane, that are molecules allowing ions in or out of the neuron. These channels are responsible for all the electrical properties of neurons, and in particular for the spike generation. There are many types of such channels on the membrane of a neuron. Considering all channels of the same type i in the neuron's membrane, the current flowing through this family of channels is traditionally modeled by [10]:

$$I^i = g^i(t, V)(E^i - V),$$

where V is the neuron's membrane potential and E^i is the *Nernst potential* associated with this type of channel. E^i is linked to the inside and outside concentrations of the type of ion flowing through the channel, that remain constant, and thus E^i is also a constant for the channel considered. If E^i is very high, then these channels tend to *depolarize* (excite) the neuron, since I^i is always positive in this case. Conversely, if E^i is negative as compared to the neuron's resting potential, this type of channels tends to *hyperpolarize* (inhibit) the neuron. As for $g^i(t, V)$ it is a *conductance* that measures the global, instantaneous opening of the family of channels i. The bigger it is, the more current flows through the channels.

The channels that generate spikes have a very specific property: they are *voltage-dependent* [10] (hence the dependence of g^i with V in the preceding equation). We do not directly model spike generation. Thus, in our framework, $g^i(t)$ is only modulated by *external causes*: synaptic inputs of the neuron, and direct stimulation by light in the case of photoreceptors.

[6] In fact, real neurons have a spatial extent. In particular, the membrane potential of one neuron is a number $V(x, y, t)$ defined at every point (x, y) of its membrane and for every time t. This structure can induce different effects. Inhomogeneous synapse repartition on the membrane of the neuron can lead to spatially varying solutions for $V(x, y, t)$. An elongated structure such as a cortical axon can induce specific propagation times on the neuron's surface. We will not take all these effects into account.

Deriving a conductance-based model. The neuron model presented here is what we refer to as a *CIF* (Conductance Integrate and Fire) neuron. We model a minimal set of three types of conductance. One channel type represents the excitatory inputs on the neuron (corresponding to a Nernst potential above the neuron's threshold): it is noted $G^{exc}(t)$. A second channel represents the inhibitory inputs to the neuron (negative Nernst potential): it is noted $G^{inh}(t)$. Finally, some channels are constant in time, corresponding to all inert leaks in the membrane. They sum up in a constant conductance g^L, associated to a null Nernst potential. This neuron model has *two* independent inputs, $G^{exc}(t)$ and $G^{inh}(t)$. It is a standard neuron model used by [46] for example. Since the membrane of a neuron acts as an electrical capacitor, the membrane potential is then driven by the following equation:

$$c\frac{dV(t)}{dt} = G^{exc}(t)(E^{exc} - V(t)) + G^{inh}(t)(E^{inh} - V(t)) - g^L\,V(t) + I(t), \qquad (1)$$

where c is the capacity of the membrane, and $I(t)$ denotes external current inputs to the neuron, such as that provided by neighboring cells through gap junctions (Section 3.3). Equation (1) is more intuitive when normalized. Let V_{spike} be the typical value of $V(t)$ at which the neuron spikes. We change our notations so as to have all potentials ($V(t)$ and Nernst potentials) divided by V_{spike}. Furthermore, all conductances are divided by c, and $I(t)$ is divided by cV_{spike}. For these new variables, (1) writes

$$\frac{dV(t)}{dt} = G^{exc}(t)(E^{exc} - V(t)) + G^{inh}(t)(E^{inh} - V(t)) - g^L\,V(t) + I(t), \qquad (2)$$

where potentials are dimensionless, while conductances and currents have the dimension of frequencies. c has disappeared thanks to the renormalization. Furthermore, if the neuron is a spiking neuron, then a spike occurs every time $V(t)$ reaches value one.

Only ganglionar cells (and some amacrine cells) fire spikes. For these neurons, every time a spike occurs, the potential $V(t)$ is reset to value zero after the spike (potential zero being the resting point in our normalized equation). Then, after a possible absolute refractory period, (2) starts driving $V(t)$ again.

Model reduction. To better understand the filtering properties of (2), we rewrite it in the following way:

$$\frac{dV(t)}{dt} = g^{\infty}(t)(E^{\infty}(t) - V(t)), \qquad (3)$$

with:

$$\begin{cases} g^{\infty}(t) = G^{exc}(t) + G^{inh}(t) + g^L, \\ E^{\infty}(t) = \dfrac{G^{exc}(t)E^{exc} + G^{inh}(t)E^{inh} + I(t)}{g^{\infty}(t)}. \end{cases}$$

Once initial conditions are forgotten, (3) has the solution

$$V(t) = \int_{\xi=0}^{+\infty} g^{\infty}(t-\xi) E^{\infty}(t-\xi) \exp\left(- \int_{t-\xi}^{t} g^{\infty}(u) du \right) d\xi. \tag{4}$$

Equation (4) can be seen, at each time t, as the linear convolution of $E^{\infty}(t)$ with a temporal kernel $\xi \rightarrow K_t(\xi)$, that itself depends on the present time t. Indeed, one can rewrite (4) as

$$V(t) = E^{\infty} * K_t \ (t), \text{ with } \begin{cases} g^{\infty}(t) = G^{exc}(t) + G^{inh}(t) + g^L, \\ \\ E^{\infty}(t) = \dfrac{G^{exc}(t) E^{exc} + G^{inh}(t) E^{inh} + I(t)}{g^{\infty}(t)}, \\ \\ K_t(\xi) = g^{\infty}(t-\xi) \exp\big(- \displaystyle\int_0^{\xi} g^{\infty}(t-u) du \big) \ , \text{for } \xi > 0. \end{cases} \tag{5}$$

This last formulation shows that $V(t)$ is always linearly driven by $E^{\infty}(t)$, whereas the dependence with respect to the conductance $g^{\infty}(t)$ is non-linear. (And as a result, the global dependence to the inputs $G^{exc}(t)$, $G^{inh}(t)$ and $I(t)$ is also non-linear). For each t, $\xi \rightarrow K_t(\xi)$ is a low-pass filter (since it is always positive), that verifies

$$\int_{\xi=0}^{\infty} K_t(\xi) d\xi = 1,$$

as one checks easily from its definition in (5). As a consequence, $V(t)$ can be seen as a temporal averaging of input $E^{\infty}(t)$, with averaging properties depending only on the recent values of $g^{\infty}(t)$.

3.1.2 Linear Approximation with respect to the Input

Equation (2) melts down to a traditional linear integration model such as the LIF neuron (Leaky Integrate and Fire model, see e.g. [10] for a review) when the leakage term g^L is much higher than the varying conductances $G^{exc}(t)$ and $G^{inh}(t)$. In that case, the neuronal integration defined by (2) is in its **linear range**. In its linear range the CIF model (2) approaches a linear LIF model with leakage conductance g^L and input current

$$I_{\text{tot}}(t) = G^{exc}(t)\, E^{exc} + G^{inh}(t)\, E^{inh} + I(t). \tag{6}$$

Indeed, (2) now writes

$$\frac{dV(t)}{dt} = I_{\text{tot}}(t) - g^{\infty}(t)\, V(t) \simeq I_{\text{tot}}(t) - g^L\, V(t), \tag{7}$$

and the solution from (5) writes

$$V(t) = \frac{I_{\text{tot}}}{g^L} * T_{1/g^L} \ (t), \tag{8}$$

where T_τ is the decreasing exponential kernel with time constant τ and integral one:

$$T_\tau(t) = \begin{cases} \frac{1}{\tau} \exp\left(-\frac{t}{\tau}\right) & \text{if } t > 0 \\ 0 & \text{otherwise.} \end{cases} \quad (9)$$

The static filter $\xi \rightarrow T_{1/g^L}(\xi)$ is the simplification of the time-varying filter $\xi \rightarrow K_t(\xi)$ in (5), when $g^\infty(t) \simeq g^L$.

This linear simplification of (2) is convenient to get theoretical results about filtering in the retina, since the linearity allows basic Fourier analysis. However, it is unclear whether such an approximation is totally justified. Interesting effects occurring in the retina might even be lost with this simplification[7].

3.1.3 Non-linearity in the CIF Model

The non-linearity of CIF (5), as compared to (8), occurs at two levels, with different implications.

Varying time constants. The first non-linearity is related to the temporal filtering kernel, $\xi \rightarrow K_t(\xi)$, which is not temporally static in the CIF model. Whether recent values of $g^\infty(t)$ are big or small, the potential $V(t)$ will follow the driving potential $E^\infty(t)$ very sharply in the first case, and much more loosely in the second case. For the moment, we do not take this non-linearity into account. Successive layers in the retina, and other transmission stages that also imply temporal delays (synaptic transmission, as presented in Section 3.2), will lead us to rather consider global, constant, filtering delays in our model. However, varying temporal scales for filtering have been observed experimentally, and a conductance formalism such as that of (5) could explain at least part of these observations, see Section 7.

Divisive normalization. The second non-linearity is in the expression of the driving potential itself,

$$E^\infty(t) = \frac{G^{exc}(t)\, E^{exc} + G^{inh}(t)\, E^{inh} + I(t)}{G^{exc}(t) + G^{inh}(t) + g^L}. \quad (10)$$

Since $V(t)$ follows $E^\infty(t)$, (10) implies that $V(t)$ corresponds to a divisive scaling by the two inputs $G^{exc}(t)$ and $G^{inh}(t)$: when these two inputs are large enough as compared to g^L, $V(t)$ becomes sensitive to the balance of the two inputs, rather than to their sum. More precisely, [50] estimate normalized values for E^{exc} and E^{inh} at respectively 4.6 and -0.6 in normalized units. These estimations have been made in the cortex, but are likely to be very similar in

[7] It has been recently showed that neurons are indeed in a high-conductance state *in the cortex* [12], which translates in our model by saying that g^L is not the main contribution to $g^\infty(t)$ anymore. Considering a general CIF model instead of its LIF simplification might be mandatory in this case.

the retina. Such values require, for the total input current $G^{exc}(t)E^{exc} + G^{inh}(t)E^{inh}$ to be balanced between excitation and inhibition, that $G^{inh}(t)$ be between five and ten times larger than $G^{exc}(t)$. Thus, $G^{inh}(t)$ will be the main scaling factor of $E^{\infty}(t)$ through (10). The effects of such possible normalization in the retina are mentioned in Section 7.

3.1.4 Solution with Spikes

Let us now consider spike generation (occurring in ganglionar cells and some amacrine cells) with the classical integrate and fire law: the neuron potential $V(t)$ follows (2) until it reaches the threshold value one. At this time, a spike is emitted, $V(t)$ is reset to value zero and stays there during an absolute refractory period τ_R, before following (2) again.

Such a behavior is hard to study in the general case. However, some approximation is possible when the inputs $G^{exc}(t)$ and $G^{inh}(t)$ vary much slower than $V(t)$, i.e

$$\frac{1}{G^{exc}}\frac{\mathrm{d}}{\mathrm{d}t}G^{exc} \ll g^{\infty}, \tag{11}$$

and similar for G^{inh}. (11) is derived from the fact that $g^{\infty}(t)$ gives the orders of magnitude for the temporal derivative of $V(t)$. From the retinal anatomy (see Section 4), approximation (11) appears reasonable for ganglionar cells. Successive low-pass filtering of the visual input in the first layers of the retina insure that the left-hand side term has very little power at frequencies higher than 50 Hz, while the right-hand side term is directly measured by spike train emissions in ganglionar cells, that reach $100Hz$ and even more [15].

If the approximation is valid, then the instantaneous firing rate of ganglionar cells is well approached by its expression for constant inputs G^{exc}, G^{inh} and I, that can be derived exactly from (3), leading to the expression

$$\nu \simeq \left(\frac{-Log\big(1 - \dfrac{G^{exc} + G^{inh} + g^L}{I_{\mathrm{tot}}}\big)}{G^{exc} + G^{inh} + g^L} + \tau_R \right)^{-1}, \tag{12}$$

where $I_{\mathrm{tot}} = G^{exc}E^{exc} + G^{inh}E^{inh} + I$ is the (constant) total input current to the cell. In our retinal simulations, even when $G^{exc}(t)$, $G^{inh}(t)$ and $I(t)$ vary temporally, they vary slow enough for (12) to provide good orders of magnitude for the real firing rate.

Firing rate for big input current. When the input current I_{tot} is big, the firing rate, calculated through (12), becomes asymptotically equal to:

$$\nu \simeq \left(\tau_R + I_{\mathrm{tot}}^{-1}\right)^{-1}, \tag{13}$$

a function linear with respect to I_{tot} as long as $I_{\mathrm{tot}} < 1/\tau_R$.

Difference with a classical LIF model. As a comparison, the firing rate for constant input in a LIF model, calculated through (7), is

$$\nu \simeq \left(\frac{-Log\big(1 - \frac{g^L}{I_{\text{tot}}}\big)}{g^L} + \tau_R \right)^{-1} . \tag{14}$$

The difference with CIF neurons (12) is subtle. In particular, both (12) and (14) lead to the same asymptotical expression (13) when the input current is big. Heuristically, the CIF non-linearity is more subtle in spiking neurons than in non-spiking neurons (Section 3.1.3) because both non-linear effects tend to inhibit one another when spikes are added to the process: a big total conductance $g^\infty(t)$ means fast response of the potential $V(t)$ (through kernel $\xi \to K_t(\xi)$) but smaller leading potential $E^\infty(t)$, since it is divided by $g^\infty(t)$, and as a result, the value of $g^\infty(t)$ has little influence on the firing rate of the cell.

However, there is indeed a difference between the CIF firing rate (12) and the LIF firing rate (14). In the case of the LIF neuron, the firing rate is only a function of the total input current I_{tot} whereas, in the CIF neuron, it is also a function of the total conductance of the neuron $G^{exc} + G^{inh} + g^L$. As a result, different couples (G^{exc},G^{inh}) that lead to the same linear input I_{tot}, and hence to the same firing rate in the LIF model, can lead to different firing frequencies in the CIF model, according to the value of $G^{exc} + G^{inh} + g^L$. We do not know yet if this effect is observed or not in real physiological recordings. Anyway, the CIF model predicts that this effect (couples (G^{exc}, G^{inh}) corresponding to the same linear prediction I_{tot} but to different firing rates) can only be observed for inputs moderately strong, since at strong inputs the firing rate becomes only a function of I_{tot}, through (13).

3.1.5 Conclusion for the Present Retina Model.

In its present state, our retina model (Section 4) uses only the linear approximation of the CIF model presented here, that is, uses only a classical LIF formalism. On the one hand, neurons that do not fire spikes (in the first layers of the retina) are modeled as linear integrators, equation (7). This allows us to model the spatio-temporal filtering performed by the first layers of the retina through linear Fourier analysis. On the other hand, the only spiking neurons in our present model are ganglionar cells and, since we do not model amacrine cells yet, they do not receive any inhibition. As a result, our ganglionar cells do not receive an input couple (G^{exc}, G^{inh}), which is the only way to observe effects specific to CIF formalism, as explained in 3.1.4. Hence, a LIF modeling is sufficient for ganglionar cells in the present state of the model.

However, we found necessary to introduce the more general CIF model for two reasons. First, because it provides a biological justification of the LIF formalism, as a particular working range of the CIF model, when input conductances are smaller than the leakage conductance of the cell. Second, because we believe that, in the first, non-spiking layers of the retina, the non linearity induced by a CIF formalism (Section 3.1.3) could provide an explanation for non-linearities experimentally observed in a real retina, see Section 7.

We now present a model for synaptic transmission in a non-spiking network.

3.2 Modeling Chemical Synapses

In this section we settle a model for the chemical synapse from a pre-synaptic neuron, noted A, to a post-synaptic neuron, noted B. In a conductance-driven neuron framework, this means studying the conversion from pre-synaptic membrane potential $V_A(t)$ to a conductance signal $g_{A\to B}(t)$ in the post-synaptic membrane, that can be either excitatory or inhibitory. At the biological level [10], post-synaptic neuron's synaptic inputs sum up to provide both excitatory and inhibitory signals[8]:

$$\begin{cases} G_B^{exc}(t) = \displaystyle\sum_{\text{pre-synaptic excitatory A}} g_{A\to B}^{exc}(t) \\ G_B^{inh}(t) = \displaystyle\sum_{\text{pre-synaptic inhibitory A}} g_{A\to B}^{inh}(t) \end{cases} \tag{15}$$

Then, equation (2) of the previous section drives $V_B(t)$ as a function of $G_B^{exc}(t)$ and $G_B^{inh}(t)$, i.e. as a function of all pre-synaptic potentials $V_A(t)$.

The goal of this section is to provide a realistic synaptic model as a background to all our calculations involving chemical synapses, with different possible levels of simplification. Our synaptic model is reduced to its linear simplification for synapses in the OPL. On the contrary, the synapses from bipolar cells to ganglionar cells are modeled with their possible non-linearities.

Modeling of a synapse requires two successive steps. First, to model how $V_A(t)$ is linked to neurotransmitter release $N_{A\to B}(t)$ in the synaptic cleft. Second, to link this neurotransmitter release to conductance openings in receptors of the post-synaptic neuron, $g_{A\to B}(t)$. We start with the latter question, using the traditional modeling found for example in [10].

3.2.1 Simple Model for a Synaptic Receptor

We limit ourselves to the modeling of a single-neurotransmitter-binding, ionotropic, receptor channel such as $AMPA$ or $GABA_A$, although many other receptors can be found in the retina[9].

Whatever type of channel considered, the global conductance induced by the opening of this kind of channels approximately writes:

$$g_{A\to B}(t) = G_{\max} P(t), \tag{16}$$

where $P(t)$ is the time-dependent probability that one receptor channel is open, and $G_{\max}$ is the maximal conductance between neurons A and B, proportional to the number of receptors

[8] Even more than a biological fact, this is a basic *electrical* relation describing conductances in parallel.

[9] for example, the metabotropic receptors allowing ON-bipolar cells to be depolarized when cones are inhibited (meaning light ON – see Section 4.1.1), although cones only release glutamate, which is a traditionally excitatory neurotransmitter.

on B's membrane. This last number is very important, since it is a measure of the *synaptic weight* between the two neurons: the stronger this number is, the more impact A can have on B. (16) results from a statistical counting of the number of open post-synaptic receptors; it supposes that the number of receptors is large enough to calculate a reliable mean.

In the case of simple receptors, $P(t)$ is in turn driven by:

$$\frac{\mathrm{d}P(t)}{\mathrm{d}t} = \alpha(t)(1 - P(t)) - \beta\, P(t). \tag{17}$$

In this equation, $\alpha(t)$ is the instantaneous density of probability that a closed molecule fixates a neurotransmitter, and thus opens. It is highly dependent on the neurotransmitter release by the pre-synaptic neuron: the more transmitters are available, the bigger the probability that the receptor fixes one. This is why $\alpha(t)$ displays a dependence in t. The most classical claim is that $\alpha(t)$ is *directly proportional to the concentration of neurotransmitters in the synaptic cleft*[10]. This writes

$$\alpha(t) = \kappa N_{A\to B}(t).$$

On the contrary, β is the instantaneous density of probability that an open channel releases its neurotransmitter and comes back to closed state. This, in turn, is a constant only dependent on the chemical properties of the two molecules. Note that $\alpha(t)$ as well as β have the dimension of an inverse time: they define time constants for the evolution of P. β uniquely depends on the type of channel considered. For fast channels such as $AMPA$ or $GABA_A$, β^{-1} is around 5 ms. For slow channels like $NMDA$, it is bigger than 100 ms [10].

Interestingly, $P(t)$ is linked to $\alpha(t)$ by an equation similar to (2). As a result, the solution to (17) is formally identical to (5), and writes:

$$P(t) = P^{\infty}(t) * K_t(t), \text{ with } \begin{cases} \gamma(t) = \alpha(t) + \beta \\ P^{\infty}(t) = \dfrac{\alpha(t)}{\gamma(t)} \\ K_t(\xi) = \gamma(t-\xi)\exp\big(-\int_0^{\xi}\gamma(t-u)\mathrm{d}u\big) \text{ , for } \xi > 0 \end{cases} \tag{18}$$

The two non-linearity at this stage of synaptic transmission are the same as those described in 3.1.3. The most important seems the possible normalization:

$$P^{\infty}(t) = \frac{\alpha(t)}{\alpha(t) + \beta} \tag{19}$$

If $\alpha(t)$ becomes bigger or comparable to β, then $P^{\infty}(t)$ gets close to 1, followed by $P(t)$. The synapse is said to **saturate**, as represented in Figure 8 (B).

[10] This modeling also applies to receptors that have to bind with multiple neurotransmitters to be opened. If a channel is open after binding of k neurotransmitters, then $\alpha(t)$ will be proportional to $N_{A\to B}(t)^k$.

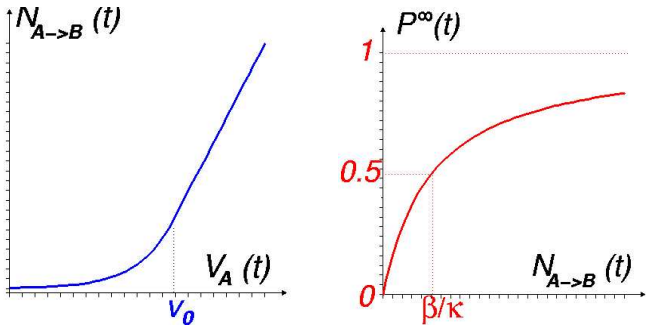

(A) Neurotransmitter release (B) Receptor saturation

Figure 8: (A) A smooth rectification/amplification links pre-synaptic potential with neurotransmitter release in the synaptic cleft. The offset on the abscissa axis, given by potential v_0, is an unknown parameter. (B) A saturation links neurotransmitter release to conductance opening, through (19). This figure represents $P^\infty(t)$ as an instantaneous transformation of $N_{A\to B}(t) = \alpha(t)/\kappa$.

3.2.2 Neurotransmitter Release

We are now left with our second issue (the first, chronologically in the synapse): link $V_A(t)$ with neurotransmitter release, $N_{A\to B}(t)$, and thus to $\alpha(t)$ in the previous equation. We make the basic assumption that $N_{A\to B}(t)$ is proportional to $V_B(t)$ in some 'linear' range, and smoothly rectified in a 'small signal' range, a behavior that qualitatively looks like that of Figure 8 (A).

Such a hypothesis is natural, and empirically justified by the fact that some ganglionar cells in the retina *do* perform quasi-linear filtering [24], which requires the possibility for synaptic transmission to work at a linear regime.

What are typical values of $N_{A\to B}(t)$? In other words, what is the amplification factor for ordinates in Figure 8 (A)? This knowledge tells us whether the synapse is saturated or not, through (19), when comparing $\alpha(t) = \kappa N_{A\to B}(t)$ with β. To approximate $\alpha(t)$, we take as a reference the case of spiking neurons, as described in [10]: when a spike occurs, the typical order of $\alpha(t)$ (for glutamate release) is around $2000Hz$ during approximately 1 ms, the duration of the spike. If $\alpha(t) = \kappa N_{A\to B}(t)$ is considered proportional to $V_A(t)$ (Figure 8 (A)), and grossly supposing that a spike implies variations of $V_A(t)$ about 10 times bigger than those below threshold, then typical orders for $\alpha(t)$ in non-spiking networks should be around $200Hz$, that is precisely the typical value of β in $AMPA$ receptors.

From these rough approximations, we conclude that synaptic saturation might become sensible in retinal synapses, which leads us to propose a generic synaptic model that *can* include such saturation.

3.2.3 Towards a Synaptic Model

From the two preceding sections, a biological framework to describe the two stages of synaptic transmission in non-spiking networks is obtained. Let us now build a global model for our synapses, that qualitatively encompasses the previously described effects of rectification, saturation, and temporal delay. Logically, the total synaptic behavior should be a *composition* of the rectification/amplification function in Figure 8 (A) by the saturation function of (19) (Figure 8 (B)). After what a temporal integration must be added, described by $\xi \rightarrow K_t(\xi)$ in (18).

Considering the rectification-amplification-saturation process, how the two successive functions *scale* one after the other is not really fixed. As a result, there is no presupposed knowledge about the relative strengths of the two non-linearities (rectification and saturation). We thus parametrize the relative weight of the two non-linearities by a related parameter $\eta \in [0, 1]$.

Another unknown in this rectification process is the *working point* of neurotransmitter release. When the retina fixes a uniform dark field, all cells of a layer have basically the same membrane potential $V_A(x, y, t) = V_A^{\text{Dark}}$. Considering a layer post-synaptic to this one, what is the consequent transmitter release? We need to position value V_A^{Dark} somewhere on the abscissa of Figure 8 (A). This introduces a second parameter in the model. Finally, the amplification factor from $V_A(t)$ to $\alpha(t)$ yields a third parameter, and the total strength of the synapse, $G_{\max}$, a fourth one.

3.2.4 A Synaptic Model

Our final model for a continuous synapse thus consists of a static transmission function from $V_A(t)$ to a 'driving conductance' $g^1(t)$, that is in turn temporally low-passed to obtain $g_{A \rightarrow B}(t)$.

Static transmission function

We introduce a normalized transmission function T_η that defines the shape of the transmission from $V_A(t)$ to $g^1(t)$. Then the total transformation is given through scaling and offset parameters:

$$g^1(t) = G_{\max} \mathrm{T}_\eta \left(\frac{\lambda}{G_{\max}} (V_A(t) - v_0) \right), \tag{20}$$

where $\eta \in [0, 1]$ and T_η is the normalized transmission function defined by :

$$\mathrm{T}_\eta(x) = \begin{cases} \eta + \dfrac{\eta x}{\eta - x} & \text{if } x < 0, \\ \eta + \dfrac{(1-\eta)x}{(1-\eta) + x} & \text{if } x > 0. \end{cases} \tag{21}$$

The four parameters are the following:

- $G_{\max}$ is the total weight of the synapse.
- λ is the amplification factor of the synapse: it gives the slope of the transmission from $V_A(t)$ to $g^1(t)$ in its linear range.
- v_0 is an offset on the abscissa axis, that can be used to define the *working point* of transmission, value when the retina does not receive any visual information. If $V_A(t) = V_A^{\text{Dark}}$ without visual stimulation (not necessarily with $V_A^{\text{Dark}} = 0$), then $(V_A^{Dark} - v_0)\lambda/G_{\max}$ corresponds to the working point of the synapse on curve T_η (see Figure 9).
- Finally, η defines the global shape of the transmission function, as described now.

The function $\mathrm{T}_\eta(x)$ defines the general shape of the static transmission. It is normalized, ranging between 0 and 1, with a derivative equal to 1 in $x = 0$. The parameter η is a way to measure the different strengths of both non-linearity (the rectification in $x \to -\infty$ and the saturation in $x \to +\infty$) when composing the functions in Figure 8 (A) and Figure 8 (B).

Figure 9 displays curves of $\mathrm{T}_\eta(x)$ for different values of η. The piecewise functions defined in (21) are Michaelis-Menten functions that saturate with x^{-1}: indeed, this is the type of saturation defined by (19) and already pictured in Figure 8. Note that for $\eta = 0.5$ the function is anti-symmetrical, and that for $\eta = 0$ it performs brutal rectification.

If the variations of V are small compared to $G_{\max}/\lambda$, then (20) can be considered linear. We make this assumption for synapses in the OPL (see Figure 2), but not for the synapse linking bipolar cells to ganglionar cells in the IPL, that is explicitly modeled with its non-linearity.

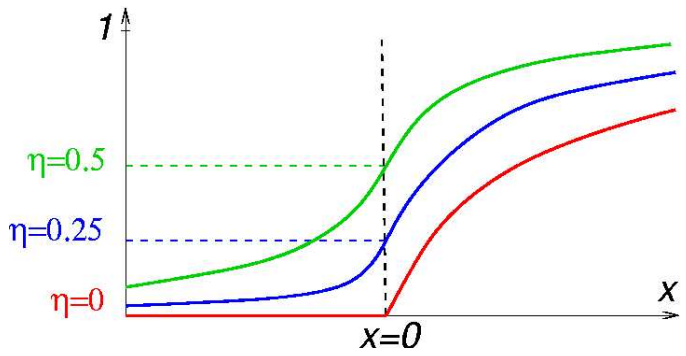

Figure 9: Graphs for three versions of function T_η, respectively $\eta = 0$ (red curve), $\eta = 0.25$ (blue curve) and $\eta = 0.5$ (green curve). T_η curves are normalized. They can be roughly considered linear between $x = -\eta$ and $x = 1 - \eta$, meaning that the length of the 'linear domain' is independent of parameter η.

About temporal delays

From (18), we see that some delay appears during synaptic transmission, through kernel $\xi \rightarrow K_t(\xi)$, with time constant grossly equal to $1/(\alpha(t)+\beta)$. Such a constant is necessarily smaller than β^{-1}.

Even for fast receptors such as $AMPA$, β^{-1} ranges around 5 ms [10], so the contribution of successive synapses to transmission delay is not negligible in primate retinas, where the total transmission delays are of a few tens of seconds (see for instance [49], or [24] in the cat retina).

Furthermore, in (18), the temporal integration kernel $\xi \rightarrow K_t(\xi)$ is not static. Although we do not take this variation into account, it could be important for receptors having low values of β (for example, $NMDA$ receptors whose time constant β^{-1} is of many tens of seconds [10]), since in this case $\alpha(t)$ would provide the main, variable, contribution to $\gamma(t)$.

Our strategy is to incorporate globally all successive temporal integration delays, at some point in our retina model. Hence, we make the approximation

$$g_{A \rightarrow B}(t) = g^1(t),$$

but remember that all synapses contribute to the total temporal filtering taking place in the retina, with orders of magnitudes depending mostly on the type of synaptic receptor considered.

3.3 Electrical Coupling between Cells

Let us introduce a final component in the modeling.

All retinal cells are linked to their neighbors of the same type by gap junctions. These junctions result in a *sharing* of the cell information conveyed by their membrane potential: for example, neighboring receptors tend to have similar membrane potentials, since ions can circulate from one receptor to another through the junctions. Figure 10 presents a 1-D view of a simple model for cell coupling, as that first introduced by [33] for horizontal cells, based on surface resistances (see also [28]), and that was later the basis for the first hardware retinal models [29].

Discrete coupling equation. We suppose that each cell is driven by a linear leaky capacity equation with leakage parameter g^L, as equation (7), and that neighboring cells are linked by a constant conductance G, modeling a simple gap junction. Cells are supposed to have homogeneous properties, meaning that g^L and G are constant for the whole network (Figure 10). Then, cell number i of the network is driven by the following equation :

$$c\frac{\mathrm{d}V_i}{\mathrm{d}t}(t) = G(V_{i+1}(t) + V_{i-1}(t) - 2V_i(t)) - g^L\, V_i(T) + I_i(t) \qquad (22)$$

When neurons are considered in the CIF framework, supposing a linear regime as in (22) means that we are in the linear conditions described in Section 3.1.2. As a consequence,

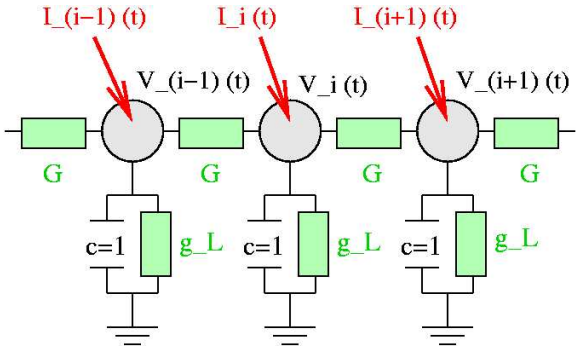

Figure 10: An electrical model for lateral coupling in a population of cells V receiving an input current I.

(22) is linear with respect to the input current $I(x, y, t)$. It can be directly solved in terms of its Fourier transform (as in [20]).

Continuous coupling equation and its solution. We prefer to assume that the cell sampling is dense enough to consider the continuous version of the preceding equation (as in [33]). As cells are separated by a spatial step s, the (serial) conductance G behave as $G = \mathcal{G}/s$, while the (parallel) conductance g^L, capacities c and input currents scale with s: $g^L = s/\tau$, $I_i(t) = sI(x, y, t)$, and $c = s$. Driving s to zero [33] then gives us the following continuous equation :

$$\frac{\mathrm{d}V}{\mathrm{d}t}(x, y, t) = \mathcal{G}\,\Delta V(x, y, t) - \frac{1}{\tau}\,V(x, y, t) + I(x, y, t). \tag{23}$$

Note that such calculations are valid for two-dimensional networks: this is the reason why we have written the spatial second derivative of V as a Laplacian function. This is a heat equation with a leakage term. It is linear with respect to I and V, and bears the solution:

$$V(x, y, t) = H \overset{x,y,t}{*} I \;\; (x, y, t), \tag{24}$$

where H, impulse response of the filter, is given by:

$$H(x, y, t) = G_{\sqrt{2\mathcal{G}t}}(x, y) \exp(-t/\tau) \tag{25}$$

with G_σ defined as the averaging Gaussian kernel of standard deviation σ:

$$G_\sigma(x, y) = \frac{1}{2\pi\sigma^2} \exp\left(-\frac{x^2 + y^2}{2\sigma^2}\right). \tag{26}$$

When $\tau \to +\infty$, the second term of the product tends towards the constant function of value 1, and H becomes the classical heat equation kernel.

H is a non-separable filter, since time t has a direct influence on the spatial part of the filtering, as defined by $G_{\sqrt{2\mathcal{G}t}}$.

The properties of filter H are considered easily in the Fourier domain:

$$\widetilde{H}(\xi_x, \xi_y, \xi_t) = \frac{\tau}{1 + \frac{\sigma^2}{2}(\xi_x^2 + \xi_y^2) - \mathbf{j}\tau\xi_t}, \tag{27}$$

where

$$\sigma = \sqrt{2\tau\mathcal{G}} \tag{28}$$

is a measure for the spatial extent of the coupling induced by $\mathcal{G}$. Equation (27) shows that H is a low-pass filter, spatially as well as temporally. Equation (27) can also be obtained as the asymptotic limit of a direct Fourier calculation starting from equation (22), for frequencies much smaller than the sampling frequency (as in [20]).

A separable approximate filter. Kernel H being non-separable is a handicap for fast numerical implementation of the coupling filter. For this reason, we approximate H by a separable filter H_{Sep}, whose spatial component is not dependent on t anymore. We simply replace filter $G_{\sqrt{2\mathcal{G}t}}$ in (25) by constant filter $G_{\sqrt{2\mathcal{G}\tau}}$, since τ defines orders for the time extent of H through the term $\exp(-t/\tau)$ in (25). With the definition for σ in (28), this writes:

$$H_{\text{Sep}}(x, y, t) = G_\sigma(x, y) \exp(-t/\tau). \tag{29}$$

One can check that the Fourier transform $\widetilde{H}_{\text{Sep}}(\xi_x, \xi_y, \xi_t)$ has the same first-order development with respect to $(\xi_x^2, \xi_y^2, \xi_t)$ as $\widetilde{H}(\xi_x, \xi_y, \xi_t)$ (equation (27)).

H_{Sep} is the kernel we will be using to model the successive intra-layer couplings in the OPL. Indeed, its separable exponential kernels allow much faster calculations than an incremental implementation of equation (22) or of convolution kernel H (equation (25)), while the resulting membrane potential values are very similar.

4 Retina Model

With the theoretical framework presented in the preceding section, we can now present the retina model itself. This section follows the order of the five layers of cells. For each, our modeling of this layer is presented. Amacrine cells are presented although we do not model them yet, in order to figure what their roles are, and which of these roles will have to be explicitly implemented in the future of this model.

These sections presenting the five layers do not take into account the spatial inhomogeneity of a foveated retina. Rather, cell densities and receptive fields are considered homogeneous, which means that we are actually considering *local* properties of retinal filtering.

Finally, one last section is dedicated to assembling all these elements in a global architecture that takes into account the radial structure of the retina.

4.1 Receptors: an Adapting Spatio-temporal Filter

Receptors possess two structurally distinct segments. The outer segment is involved in the phototransduction process, while the inner segment is a cell body very comparable to other neurons of the retina. In this section we start by describing the phototransduction process. It is an occasion to measure the effects of *light adaptation* occurring in receptors, that allows the retina to function at very different illumination levels. Then we describe the effects of electrical coupling between the receptors' inner segments.

4.1.1 Opsins and Phototransduction Cascade

Phototransduction is a series of chemical reactions that are triggered when photons are captured by a special family of molecules present in the receptors' outer segments, called *opsins*. Opsins change their structure when absorbing a single photon, or quantum of light [26]. The probability that an incoming photon is absorbed by the molecule is a function of the *wavelength* (or equivalently, of the energy) of the photon, that defines the *spectral sensitivity* of the opsin. In human retinas, opsins exist in four different versions. Only one is present in rods, but three types can be found in a cone. According to the sensitivity of the opsin it contains, a cone will be short-wavelength sensitive (S, or 'Blue', cone), medium-wavelength sensitive (M, or 'Green' cone), or long-wavelength sensitive (L, or 'Red' cone). It is the relative weight of answers for these three types of cones that defines the color we perceive in an object.

Under its excited form (when it has captured a photon), the opsin (whatever type considered) acts as a *catalyzer* for another chemical reaction, that in turn creates a catalyzer to another reaction, etc. (see e.g. [37]). In the end, the effect of this photon absorption is the *closing* of specific cation channels in the membrane, that reduce the electrical current flowing through the cell.

A catalyzed reaction has the advantage to permit the reaction of a large number of molecules, starting from very few catalyzer molecules (since these last permit the reaction but globally remain untouched by it). Thus, the three catalyzed reactions in chain allow

very few photons to close a big number of ionic channels. This is why one talks of the phototransduction *cascade*. Figure 11 represents the main chemical reactions supposed to occur during phototransduction.

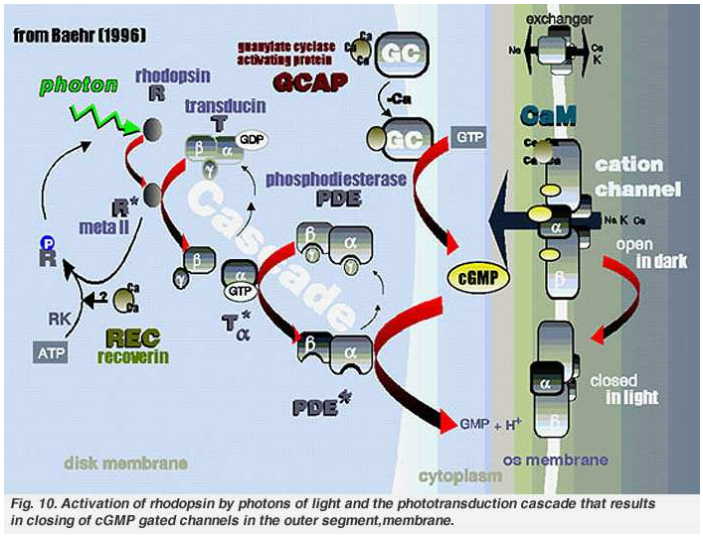

Figure 11: Principal chemical reactions occurring during phototransduction. From [37].

Note that through phototransduction, incoming light closes channels that have a positive Nernst potential, that is, *inhibits* the receptor. This inversion with the intuitive view of light exciting the receptor is not very important from a physiological point of view[11].

4.1.2 Phototransduction in Cones

The mechanism of phototransduction is not totally understood yet, quantitatively speaking. Models exist, based on classical catalyzer-modeling inherited from chemistry (Michaelis-Menten equations ...), as that proposed by [42] to explain cone phototransduction in small illumination conditions. The only experimental certitude is that, at small illuminations, the current induced in cones by phototransduction depends linearly on the received intensity

[11] The inversion is corrected at the level of ON-bipolar cells in the OPL, that are excited when receptors are inhibited, through indirect (metabotropic) synapses [26]. However, it could be important from an *energetic* point of view: rods, that are by far more numerous than cones, are generally saturated in the daytime, meaning that they are always at their maximal light absorption level. If they were to be *excited* by light, they would always have widely open channels in the daytime, forcing their ionic pumps to work at full speed all day long. On the contrary, the *inhibition* by light is a good way to save energy in rods during the daytime. Coherent with this view, rods are only connected to specific ON-bipolar cells, the only type needed to detect *increases* of the light intensity in a globally dark scene.

of light. Saturation appears for bigger intensities of received light, but it is counterbalanced by specific adaptation effects that allow the receptor to function under very different illumination conditions.

We only provide in this report a qualitative, empirical equation that summarizes our understanding of the experiments of [42] on single cones, and of [47] on populations of cones. This phototransduction equation is not implemented in our retinal program for the moment. However, it seems interesting for this report to deal with the complete retinal processing from incoming light to spikes. We qualitatively describe the opening of light-sensitive conductances in the outer segment of a cone receiving a light intensity I by:

$$G_R^{exc}(t) = G_{\max} - G_{\max}\mathrm{Sat}\left(\frac{1}{G_{\max}} I \star f_{\bar{I}}\ (t)\right). \tag{30}$$

This qualitative equation is a personal interpretation of the results of [42, 47]. It encompasses the properties of cone phototransduction as described in these two articles, but lacks validation for adaptation levels of light different than darkness. It must only be seen as our attempt to put an equation on well-known facts concerning phototransduction. The different terms in this equation are the following:

- $I(t)$ is the light intensity fed to the cone, measured for example in photons received per second.
- $\bar{I}$ is the ambient light intensity, to which the receptor has been *adapted*. It is calculated, grossly, from the light intensities presented to the receptor during its recent history, with time constants of the order of one second (for the effect of *cellular adaptation* [47]), or of one minute (for the effect of *pigment bleaching* [47]).
- $f_{\bar{I}}(t)$ is the theoretical conductance opening caused by the absorption of *one* photon, after adaptation of the cell to light conditions $\bar{I}$. We use the word "theoretical" to stress that a single photon can never be detected by a cone, even adapted to darkness [42]. Thus, $f_{\bar{I}}(t)$ must only be seen as the cone's impulse response after adaptation at illumination $\bar{I}$. Defining an impulse response for the cone makes sense, since the linearity with respect to $I(t)$ has been proved at low intensities [47] (when $I(t)$ and $\bar{I}$ are small), as in Figure 12.

  Phototransduction modeling by [42] proposes that $f_{\bar{I}}(t)$ have a *biphasic* shape, as illustrated in Figure 12, for cones in the dark ($\bar{I} = 0$). However, our personal belief is that the transient response observed for cones under dim light (Figure 12) is rather due to a feed-back from horizontal cells (see Annex B). If this should be the case, the transiency of cone responses would not yet appear at the level of light-sensitive ionic channels, that we modeled here ($G_R^{exc}(t)$ in (30)). As a result, $f_{\bar{I}}(t)$ might only be a positive 'blob', performing a simple temporal low-passing on the light input $I(t)$.
- sign $\star$ represents the linear answer of the receptor to incoming light. It means temporal convolution of $I(t)$ with function $f_{\bar{I}}(t)$. When $I(t)$ consists of polychromatic light

(general case), the sign $\star$ also includes a dot product between the light spectrum of $I(t)$ and the opsin's absorption spectrum.

- $G_{\max}$ is the maximum conductance when all light-sensitive channels are open in the receptor's membrane (as in the synaptic transmission model, Section 3.2).
- function $x \rightarrow \mathrm{Sat}(x)$ is a saturation function, whose shape is not modeled here, but that we suppose to be "normalized": it ranges between values zero and one, with a derivative of one in $x = 0$. Modeling channel saturation by a static function is a classical procedure that bears good experimental justification [47, 42]. The strength of this saturation is experimentally observed as an intermediate between exponential saturation ($x \rightarrow 1 - \exp(-x)$) and Michaelis-Menten saturation ($x \rightarrow x/(1+x)$). Note that both these functions given as examples enter the category of what we called "normalized" functions.

The general shape of this equation, $G_R^{exc}(t) = G_{\max} - \textit{something}$, is due to the fact that receptors are "reversed": incoming light causes ionic channels to *close*. Receptor saturation is illustrated in Figure 13, where we have chosen, for function Sat, one of the transmission curves T_η presented in Section 3.2.

We define the *working point* of the receptor as the term inside of function Sat:

$$x(t) = \frac{1}{G_{\max}} I \star f_{\bar{I}}\,(t). \tag{31}$$

Note that in the example of Figure 13, the working point can be negative. Indeed, there could be a number of channels that are already closed in the dark (when $I = 0$), and that contribute to a ground conductance closing of $G_{\max} - G_0$ in the dark. From the point of view of [42], these channels could also open, meaning that the cell would see "darker than dark", resulting in the undershoot of the impulse response depicted in Figure 12. In our point of view, this 'negative' part of the saturation function Sat is not necessary, since the undershoot in Figure 12 is well explained by feedback from horizontal cells, acting at the level of other conductances in the receptor's membrane. This means that in our optic, one could have directly $G_0 = G_{\max}$.

Linear range versus saturation. If the working point $x(t)$ in (31) is close enough to 0, as compared to the normalized saturation value of 1, then the receptor is in its linear range, meaning that its response can be approximated by:

$$G_R^{exc}(t) \simeq G_0 - I \star f_{\bar{I}}\,(t), \tag{32}$$

where G_0 is the value of G_R^{exc} when $I = 0$ (see Figure 13). If linearity is verified, then the receptor performs linear spatio-temporal shaping of the illumination signal, through function $f_{\bar{I}}(t)$. This is not always the case in real receptors. Some *response compression* is indeed observed in light-induced currents at high illumination, due to the fact that the receptor is not in the linear range of its saturation curve anymore [47].

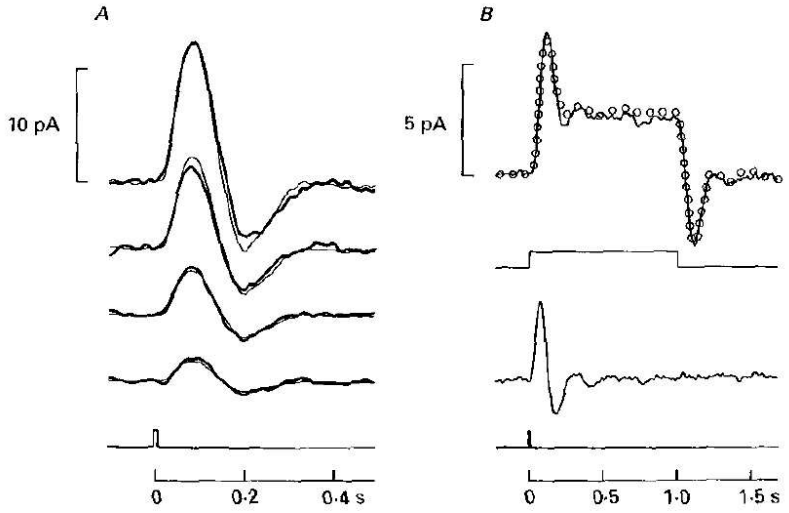

Figure 12: Current flowing through a red-sensitive cone, that has been dark adapted, in response to flashes of light. (A) Response of the cone to brief flashes of increasing intensities. Short duration of the flash insures that the subsequent answer has a shape close to the theoretical impulse response of the system $f(t)$. The response is linear. (B) Measured answer to a step of light, and predicted linear answer using impulse response $f(t)$ (circles). Temporal linear summation is observed. Note that even after initial onset, the cone still has a positive answer: $f(t)$ is not totally transient, it has a strictly positive temporal integral. In the optics of [42], $f(t)$ is proportional to the light-induced conductance opening $f_{\bar{I}}(t)$ (see text), whereas in our optics the biphasic shape of $f(t)$ is created by a feedback from horizontal cells. From [42].

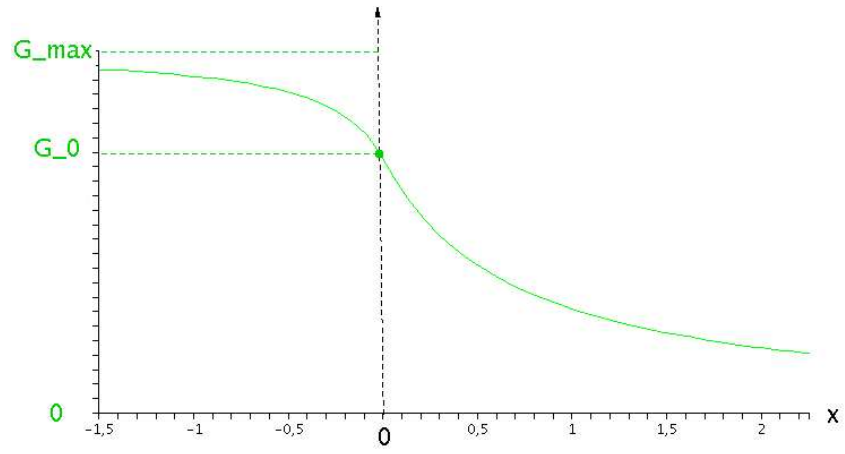

Figure 13: Our model for conductance opening by phototransduction in receptors. Variable $x(t)$ is the *working point* of the receptor, as defined from (31) by $x(t) = \frac{1}{G_{\max}} I \star f_{\bar{I}}\ (t)$.

Adaptation to light. As reported by [42, 47] for example, a global *scaling* of the receptor activity occurs as a function of its recent illumination conditions, that we have formally noted $\bar{I}$ in this section. This is what allows our retina to see at very different illumination levels, although values for $I(t)$ can vary within a factor 10^9 according to the time of day.

The most simple approximation, known as the Weber-Fechner relation, is that the sensitivity of the cell scales with $\bar{I}^{-1}$. It means that the order of magnitude of the cone impulse response $f_{\bar{I}}(t)$ varies with $\bar{I}^{-1}$. However, distinct sources of light adaptation coexist in receptors, with different time scales. One is *cellular adaptation* based on ion Ca^{2+} [37, 42], with time constant around one second. The other is *pigment bleaching*, an inactivation of the receptors' opsins under bright illumination, with time constant of around one minute [42].

In our formalism of (30), these two adaptation phenomena provide the global *scaling* of function $f_{\bar{I}}(t)$ as a function of $\bar{I}$. But the *shape* of function $f_{\bar{I}}(t)$ might also depend on background illumination $\bar{I}$, a knowledge that we lack at this point of our bibliography, although [42] provide some results.

For all these reasons, our present retinal model does not consider phototransduction explicitly. We assume that input images to our model directly represent $G^{exc}(x, y, t)$, the conductance opening in photoreceptors as caused by phototransduction.

4.1.3 Phototransduction in Rods

The experiences of [42, 47] were pursued on cones. Similar studies exist for rods in the literature [27, 3]. But here we only present general reflections, that lack bibliographical validation. This section is just the occasion for us to play with the parameters introduced in equation (30) while presenting the general physiology of rod answers. We make the hypothesis that (30) is also an acceptable modeling for light-induced currents in rods. Then, some quantitative differences would exist in the values of the parameters, reflecting the physiological differences between rods and cones.

First, rods are globally *much more sensitive* to light than cones, and saturate at much lower illuminations as well [27, 3]. Thanks to a more easily excitable opsin (rhodopsin), and to different magnitudes of catalyzer concentrations in the phototransduction cascade, rods can be sensitive to as little as *one* received photon [38]. And such sensitivity is indeed necessary at night. In equation (30), this would result in a drastically bigger scaling for function $f_{\bar{I}}$, as measured in conductance opening per received photon.

Second, the shape of their response to flashes of light is also different. It is always a monophasic 'blob' (meaning, in our optic, that there is a less important feedback from horizontal cells than in cones), and its time decay is much longer than in cones. Both facts combine to make fast intensity changes hard to perceive by rods (no strong current at onset of intensity change as in cones (Figure 12), and temporal 'blurring' due to the long-lasting impulse response)[12].

Finally, although light adaptation in rods also exists, it does not occur in such a wide range as for cones, and cannot prevent saturation past some illumination level, grossly corresponding to daylight. This would require different parameters for the scaling of $f_{\bar{I}}(t)$ with $\bar{I}$.

In these three first sections we have presented the general characteristics of phototransduction in the outer segments of receptors. To complete our overview of the receptor layer in the retina, we model the electrical coupling occurring between different receptors' inner segments.

4.1.4 Receptor Coupling

Receptor inner segments are linked one to another through gap junctions. This coupling is at the root of the spatial extent of bipolar cells' *"center"* receptive field (see Section 4.3). We can apply the linear model of Section 3.3 to receptor coupling, with an input current defined as the light-induced current caused by phototransduction:

$$I(x, y, t) = G_R^{exc}(x, y, t)E^{exc},$$

where $G_R^{exc}(x, y, t)$ is the light-induced conductance opening described in the preceding section, for the receptor in (x, y). Note that, in our CIF formalism of Section 3.1, this is justified

[12] this is the reason for which movements are much harder to perceive at night, for example when playing ball games

only if receptors are in their linear range as described in Section 3.1.2. Considering one receptor located in (x,y), the linear approximation will be justified if the leakage conductance of one receptor's membrane g^L is bigger than the light-dependent term $G_R^{exc}(x,y,t)$. We have no proof that this is the case in a real retina, but it allows us to apply results of Section 3.3 for linear coupling.

We decompose $G_R^{exc}(x,y,t)$ as its constant value in the dark G_0 (as defined in Section 4.1.2) plus its fluctuation $\Delta G(x,y,t)$ provoked by visual stimuli:

$$G_R^{exc}(x,y,t) = G_0 + \Delta G(x,y,t).$$

Then, using the approximate kernel defined in equation (29), the filtering from (continuous) input signal $G_R^{exc}(x,y,t)$ to potential $V_R(x,y,t)$ of the receptor layer is given by:

$$V_R(x,y,t) = V_R^0 + A_R \, \Delta G \overset{x,y,t}{*} H_R \;\; (x,y,t). \tag{33}$$

where H_R is the following separable, averaging filter (its spatio-temporal integral is equal to 1) :

$$H_R(x,y,t) = G_{\sigma_R}(x,y) T_{\tau_R}(t),$$

where G_σ is the Gaussian kernel of standard deviation σ and integral one defined in (26), and T_τ is the decreasing exponential kernel of time constant τ and integral one, defined in (9). τ_R is defined in Section 3.3 as the membrane time constant of receptors. $V_R^0 = G_0 \tau_R E^{exc}$ is the receptors' potential in the dark. A_R is the gain of the filter and is equal to $\tau_R E^{exc}$. The effect of receptor coupling is that the visual message obtained by phototransduction in the outer segments of receptors is temporally and spatially low-passed. The next layers of the visual pathway, horizontal cells, add further low-passing to the visual signal. Also note that, when writing (33), we implicitly supposed that the only input current to receptors is caused by light-sensitive channels. It is in fact well-known that a feedback from horizontal cells creates a second source of current on receptors' inner segments. We consider modeling this feedback in Annex B.

4.2 Horizontal Cells: Local Averagers

In turn, receptors transmit their potential values to horizontal cells through chemical synapses. Using the continuous synapse modeling that we proposed in Section 3.2.4, the conversion from receptor potentials $V_R(x,y,t)$ to synaptic current in the horizontal cells is not necessarily linear, since it implies possible rectification of the signal, saturation of the synapse, plus a temporal low-pass averaging due to neurotransmitter release time.

However, we will suppose here that we are in the linear range of synaptic transmission, to simplify calculations and keep our linear formalism. We also suppose that receptors transmit their signal to horizontal cells in purely feed-forward manner. There actually exists a feedback from horizontal cells to receptors. We show in Annex B that the feedback from horizontal cells does not significantly change the filtering at the output of the retina.

Then, the filtering from $G_R^{exc}(x,y,t) = G_0 + \Delta G(x,y,t)$ to $V_H(x,y,t)$ can be written:

$$V_H(x,y,t) = V_H^0 + A_H \, \Delta G \overset{x,y,t}{*} H_R \overset{t}{*} T_{\tau_{\text{Syn}}} \overset{x,y,t}{*} H_{R\to H} \ (x,y,t), \tag{34}$$

where T_τ and G_σ still denote respectively averaging exponential and Gaussian filters. In (34), the first convolution product gives the receptor layer potential $V_R(x,y,t)$ as defined in (33). Then, temporal convolution with $T_{\tau_{\text{Syn}}}$ is a reminder that additional delay τ_{Syn} can occur through the synapse, as explained in Section 3.2.4. Finally, $H_{R\to H}$ is the same type of separable filter as in (29):

$$H_{R\to H}(x,y,t) = G_{\sigma_h}(x,y) T_{\tau_h}(t),$$

where τ_h is the typical time constant of the horizontal cells' membrane, and σ_h the scale for spatial coupling between horizontal cells as defined in Section 3.3. V_H^0 is the constant potential 'in the dark', resulting from receptors' resting potential V_R^0 through synaptic transmission. A_H is the total gain from ΔG to V_H. It writes $A_H = A_R \lambda_{\text{Syn}} E^{exc} \tau_h$, where λ_{Syn} is the synaptic amplification from pre-synaptic potential to post-synaptic conductance opening.

How can the filter in (34) be easily modeled? Separating spatial convolution from temporal convolution in equation (34), we find that the total filtering provided by horizontal cells is a separable filter, of spatial component:

$$G_{\sigma_R} \overset{x,y}{*} G_{\sigma_h} \ (x,y),$$

and of temporal component:

$$T_{\tau_R} \overset{t}{*} T_{\tau_{\text{Syn}}} \overset{t}{*} T_{\tau_H} \ (t),$$

where the G_σ and T_τ are respectively spatial Gaussian kernels and temporal exponential kernels.

The spatial component is straightforward: the convolution of two Gaussians gives another Gaussian kernel, of standard deviation $\sigma_R + \sigma_h$. As for the second component, it is the multiple convolution of exponential decays. Such a filter is described in Annex A. It always corresponds to a low-pass positive kernel, with a 'blobby' shape that can be approximated by function $T_{\alpha,\tau}(t)$ described in Annex A. It is a function that reaches its maximum value at time $\alpha\tau$, before decaying with time constant τ. It induces a total delay of value $(1+\alpha)\tau$.

Finally, we approximate the response of the horizontal layer of (34) by:

$$V_H(x,y,t) = V_H^0 + A_H \, \Delta G \overset{x,y,t}{*} H_H \ (x,y,t). \tag{35}$$

where H_H is the averaging filter:

$$H_H(x,y,t) = G_{\sigma_H}(x,y) T_{\alpha_H,\tau_H}(t).$$

Spatial extent constant σ_H is defined as $\sigma_R + \sigma_h$. As for parameters α_H and τ_H, they depend on the different time delays involved. If all synaptic time constants are small (fast

synaptic receptors), then α_H should be close to 1 and τ_H close to τ_R, meaning that the main contribution to T_{α_H,τ_H} are the two cellular integration filters, with time constants $\tau_R \simeq \tau_h \simeq 1/g^L$.

On the contrary, if synaptic transmission between cones and horizontal cells is slow (with a big time constant $\tau_{\text{Syn}} \simeq 100$ ms), then it might become the main contribution to T_{α_H,τ_H}, leading to $\alpha_H \simeq 0$ and $\tau_H \simeq \tau_{\text{Syn}}$. See Annex A for more details.

4.3 Bipolar Cells: Band-pass Filters

The last step in the OPL is the simultaneous integration of receptor and horizontal signals by bipolar cells, both signals having opposite polarities. OFF-bipolar cells are depolarized (excited) by receptors and hyperpolarized by horizontal cells. This setup makes OFF-bipolar cells sensitive to sudden *decreases* in luminosity, since receptors themselves are excited by light decreases. On the contrary, ON-bipolar cells are hyperpolarized by receptors and depolarized by horizontal cells, which makes them sensitive to sudden *increases* in luminosity[13].

4.3.1 Bipolar Linear Filter

A conductance-based formalism for bipolar cells leads us directly to section 3.1.1 and the CIF model, with two conductance inputs, one excitatory and the other inhibitory, and in particular to equation (5) that describes the evolution of the corresponding cells' membrane potential:

$$V(t) = E^\infty * K_t\ (t),\ \text{with}\ \left\{\begin{array}{l} g^\infty(t) = G^{exc}(t) + G^{inh}(t) + g^L, \\ \\ E^\infty(t) = \dfrac{G^{exc}(t)E^{exc} + G^{inh}(t)E^{inh}}{g^\infty(t)}, \\ \\ K_t(\xi) = g^\infty(t-\xi)\exp\big(-\displaystyle\int_0^\xi g^\infty(t-u)du\big)\ \text{, for } \xi > 0. \end{array}\right.$$

As stated in section 3.1.2, such an integration model can be considered linear with respect to its input if the leakage conductance g^L is much bigger than the varying, signal-induced conductances $G^{exc}(t)$ and $G^{inh}(t)$, in which case the driving potential $E^\infty(t)$ can be considered as a linear weighting of the two inputs. We suppose that this "big g^L" condition indeed applies. To insure linear transmission, we must also suppose that the different synapses to bipolar cells are in their linear range.

In this case we can apply the same principle that has led us from receptor filter H_R (33) to horizontal cell filter H_H (35). We include temporal delays induced by synaptic transmission and signal integration in bipolar cells (whose time constant, defined by kernel $\xi \to K_t(\xi)$

[13]Receptor synapses only release glutamate, an excitatory neurotransmitter. For this reason, the hyperpolarisation of ON-bipolar cells by cones requires a second-order synaptic receptor molecule (not a simple neurotransmitter-binding channel), called a metabotropic receptor. This property confers ON-Bipolar cells with a somewhat slower response to light changes.

in the preceding equation, is approximately constant and equal to $(g^L)^{-1}$), directly in the previously defined filters H_R and H_H (defined respectively in (33) and (35)). Coupling in the bipolar cell layer can also be added as we have performed for the horizontal layer. As a result, we write the linear relation between light induced conductances and bipolar cell potential as:

$$\begin{aligned} V_{\text{Bip}}(x,y,t) &= V^0_{\text{Bip}} + A_C \, \Delta G \overset{x,y,t}{*} H_{\text{Bip}} \ (x,y,t), \\ \text{with :} \quad & \begin{cases} H_{\text{Bip}} = H_C - wH_S, \\ H_C(x,y,t) = G_{\sigma_C}(x,y) T_{\alpha_C,\tau_C}(t), \\ H_S(x,y,t) = G_{\sigma_S}(x,y) T_{\alpha_S,\tau_S}(t). \end{cases} \end{aligned} \tag{36}$$

This equation sums up our retinal model as far as the OPL. H_C and H_S are averaging spatio-temporal filters defined exactly the same way as we had defined H_H, the horizontal cell filter. They correspond to the *center* and *surround* part of the bipolar cells' receptive fields, and arise respectively from the receptor signal and from the horizontal cells signal.

A_C is the total gain for the *center* part of the filter; it could be calculated as a product of several Nernst potentials, synaptic amplification factors and time constants. If A_C is positive then one models an ON bipolar cell. If it is negative, one models an OFF bipolar cell. V^0_{Bip} is the ground bipolar cells depolarization in the dark.

More importantly, w is the *relative weight* of *center* and *surround* inputs. It is calculated as the ratio of the total gain for *surround* signal, A_S, with the *center* gain A_C: $w = A_S/A_C$. w rules the band-pass properties of the bipolar cell. We suppose that $0 < w < 1$.

4.3.2 Study of the Filter

Totally band-pass filter. For $w = 1$, the bipolar filter H_{Bip} is *totally band-pass*, in this sense that a spatially and temporally constant zone of the image will not evoke any response of the bipolar cell (that is, $V_{\text{Bip}} = V^0_{\text{Bip}}$), as one can check easily since both filters H_C and H_S are normalized.

In this case, the spatio-temporal properties of $H_{\text{Bip}} = H_C - H_S$ are best seen through the following decomposition, directly obtained from (36):

$$H_{\text{Bip}}(x,y,t) = \left[G_{\sigma_C} - G_{\sigma_S}\right](x,y) T_{\alpha_C,\tau_C}(t) + G_{\sigma_S}(x,y) \left[T_{\alpha_C,\tau_C} - T_{\alpha_S,\tau_S}\right](t). \tag{37}$$

The first term of this sum is a spatially band-pass filter, while the second term is a temporally transient filter. The first term insures that a temporally static but spatially non-uniform zone of the image (e.g. an edge in a static image) *will* evoke some response of the bipolar cell, even long after onset of the image. Conversely, the second term insures that a spatially uniform, but time-varying intensity pattern, will also evoke response in ganglionar cells. These two properties are obtained thanks to the non-separability of the bipolar filter, $H_C - wH_S$.

Partially band-pass filter. If $w < 1$, the bipolar cell will respond to a mixture of the (spatio-temporally) transient filter $H_C - H_S$ and of the (spatio-temporally) sustained filter H_C. Indeed, in this case, the bipolar filter writes:

$$H_{\text{Bip}} = H_C - wH_S = (1-w)H_C + w\big[H_C - H_S\big]. \tag{38}$$

The second term of the sum is the totally band-pass filter studied in the previous paragraph, while the first term is only proportional to the *center* signal, that is a low-pass filter.

What are plausible values for w as inspired from experience? If the bipolar filter is totally transient ($w = 1$), all objects that are spatially uniform and temporally static would not be coded at all. In everyday life, our eyes are never really static[14], so totally static image presentations before our eyes are hard to simulate. However, we do not go blind when staring for a long time at a totally white wall. This implies, whether that some low-pass component is also present in the answer of ganglionar cells (meaning $w < 1$ in our model), whether that the brain manages to reconstruct a scene only from its edges. Such total reconstruction from the edges seems a very useless complication for the brain: intuitively, a weak 'ground signaling' of the scene should also be helpful, yielded by a weight $w < 1$ in our model.

Anyway, the 'ground' component of bipolar cells is certainly less important than its 'band-pass' component for scene analysis. Furthermore, from a strict filtering point of view, the gain of filter H_C is much bigger than that of the *difference* of filters $H_C - H_S$. This means that, for the total filter to display an sensible mixture of both 'ground' and 'band-pass' component, w must be very close to 1 (higher than 0.9). Such values for w are experimentally verified in retinal measurements [15], and lead to a correct balance of 'ground' and 'band-pass' filters when simulating an array of ganglionar cells (Section 5).

w being very close to one, the 'band-pass' component of the cells has a sensible impact on the total filtering, temporally as well. As a result, 'weird' effects do appear when looking at totally static images, that elicit way less response from the retina[15].

4.3.3 Transient and Sustained Bipolar Cells

Apart from the classical ON and OFF distinction, another distinction exists between different bipolar cell types. It concerns their *temporal scale* of filtering, which we have resumed in our model by variables $(1+\alpha_C)\tau_C$ and $(1+\alpha_S)\tau_S$. As measured by [16], some bipolar cells have *transient* (high-pass) answers to visual stimulation, while others have *sustained* (low-pass) answers.

We have included in the total temporal delaying the delay caused by temporal integration occurring at the synapses from cones and horizontal cells to bipolar cells. Our model for bipolar cells could explain transient and sustained cells according to the nature of the excitatory synapses to the bipolar cell. Transient cells would be stimulated by fast synaptic receptors (such as $AMPA$ or $GABA_A$), whereas sustained cells would be stimulated by slower receptors.

[14] During visual fixation, small and periodic movements of the eyes occur, known as "microsaccades".

[15] It has been experimentally observed that, when the eyes' microsaccades are blocked, the visual perception is, at least faded, and maybe totally suppressed, tending towards a gray field.

In the first type of cells (transient), synaptic integration time would be relatively short, and only contribute of an order of 10 ms to the values for $(1+\alpha_C)\tau_C$ and $(1+\alpha_S)\tau_S$. As a result, $(1+\alpha_C)\tau_C$ and $(1+\alpha_S)\tau_S$ remain quite different (and short), and the filter truly performs a temporally band-pass filtering. Such cells will be useful for applications as movement detection, since their maximum answer is provoked by temporally band-pass stimuli.

In the second type of cells (sustained), slow receptors (e.g. $NMDA$ or $GABA_B$), whose fixation time is much longer (around 100 ms), would result in long delaying times for *center* and *surround* (respectively $(1+\alpha_C)\tau_C$ and $(1+\alpha_S)\tau_S$). Furthermore, relatively speaking, these two delays would now be comparable. Taking the approximation $(1+\alpha_C)\tau_C \simeq (1+\alpha_S)\tau_S \simeq \tau$ for these cells, one finds that their filter can be approximated by:

$$H_C - wH_S(x,y,t) \simeq \left[G_{\sigma_C} - wG_{\sigma_S}\right](x,y)T_\tau(t),$$

that is, a separable filtering that corresponds to a spatial difference of Gaussians, temporally averaged with the (long) time constant τ. In our model, these cells can still have any spatial filtering property, depending on weight w. But on the temporal side, they are low-pass cells, sensible to slow features only.

4.4 Spike Generation in the IPL

We now model the second layer of processing of the retina, the IPL. Its role is much less understood. Each cell type of the IPL (bipolar, amacrine and ganglionar) exists under several subtypes, much more than cones or horizontal cells. Cells with the greatest diversity are amacrine cells. No less than 29 different subtypes of amacrine cells exist [31], with such different receptive field sizes and properties that no common modeling for all amacrine cells can be envisaged. The only role of the IPL in the present model is to convert the continuous bipolar signal in a series of emitted spikes, by a discrete array of ganglionar cells. This spiking procedure is directly inherited from neuron modeling in Section 3. After we present the spiking procedure, we briefly review the possible roles of amacrine cells and how they could be added tot the present model.

4.4.1 Ganglionar Cells

Ganglionar cells are modeled as CIF integrate-and-fire neurons (Section 3.1). This requires they receive their input from bipolar cells in the form of an excitatory conductance. Contrary to synapses in the OPL (Sections 4.1.4.2,4.3), the excitatory synapse from bipolar cells to a ganglionar cell is modeled *with its possible non-linearities.*

Let there be a ganglionar cell i located in (x_0, y_0) on the retina. We calculate the excitatory conductance on ganglionar cell i through the synaptic modeling of (20):

$$G_i^{exc}(t) = G_{\max} \mathrm{T}_\eta \left(\frac{\lambda}{G_{\max}} (V_{\mathrm{Bip}}(x_0, y_0, t) - v_0) \right). \tag{39}$$

Equation (39) performs possible rectification and saturation of the signal from bipolar cells, according to the values of the four parameters λ, v_0, $G_{\max}$ and η (see Section 3.2.4).

Then, excitatory conductance $G_i^{exc}(t)$ is fed to the ganglionar cell i according to the spiking procedure defined in Section 3.1.4. Note that, since our model displays no inhibitory input on ganglionar cells, this procedure shows little qualitative differences with a classical LIF spiking procedure (see Section 3.1.5). However, the CIF formalism might become more interesting as compared to a LIF formalism when amacrine cells, that are inhibitory, are modeled.

Two sources of noise can be added in the spiking process: first, a Gaussian correlated noise is added to the ganglionar cell's theoretical potential as derived from equation (5). This noise sums up the effects of synaptic noise in the whole retinal processing. Second, a Gaussian variation is displayed on the duration of the refractory period following each spike. These two sources of noise allow generated spike statistics to highly resemble those of real recorded cells [24]. We use these two sources when simulating single ganglionar cells (Section 5.2).

4.4.2 Amacrine Cells : further Adaptation and Signal Shaping

Amacrine cells are not modeled for the moment. Because of their diversity, modeling them as a whole is impossible. Each subtype should be modeled with its specific effect on signal processing. However, all amacrine cells share one property: they are inhibitory cells, receiving excitatory input from bipolar cells and/or ganglionar cells (depending on the amacrine subtype considered). Being inhibitory cells makes them regulators of the firing of ganglionar cells. Although many distinctions exist between amacrine subtypes, they all fit in two broad categories: *short-range* and *long-range* amacrine cells [31]. The first have small dendritic trees and consequent receptive fields, about the size of bipolar cell receptive fields. As a consequence, they are involved in *local* shaping of the ganglionar output, and in particular in temporal shaping. On the contrary, long-range amacrine cells can cover distances in the retina of several millimeters, and would be involved in synchronization of ganglionar spikes, as well as in contrast adaptation [31].

Amacrine cells do not have the same connectivity as horizontal cells in the OPL. Along with possible gap junctions between certain subtypes of amacrine cells, one can also find *inhibitory* chemical synapses linking neighboring amacrine cells [26], a connectivity that results in different filtering properties than coupling through gap junctions, and requires further modeling.

Let us rapidly review some of the properties experimentally observed for particular amacrine cells.

Temporal shortening of ganglionar responses. Amacrine cells being inhibitory, their connection to ganglionar cells tends to reduce the firing of these cells. Populations of amacrine cells have been observed [35] that are responsible for cutting the answer of some ganglionar cells, making these ganglionar cells more transient. The signal traveling through this class of amacrine cells is temporally delayed by membranar integration and synaptic

transmission, resulting in a band-pass behavior for the subsequent ganglionar cells, by the same mechanism of delayed inhibition than for bipolar cells and the OPL (Section 4.3).

Precisely, the biological interest of such a class of amacrine cells is not obvious, since temporal band-passing is already supposed to occur in the OPL. One can hypothesize that, by having two successive steps of lateral inhibition, the retina is more robust to different types of stimuli. For example, the second inhibition due to amacrine cells, could help in shortening the response of ganglionar cells situated on image edges, since the non-separability of filtering in the OPL implies that spatial edges are not much temporally band-passed at the level of bipolar cells. Also, one should not forget that, spatially, the filtering occurring in a layer of amacrine cells can have different effects than in the OPL, because of reciprocal inhibitory contacts between amacrine cells.

Delayed inhibition seems particularly necessary in shaping the response of Parasol (α-type) ganglionar cells, not modeled in the present report. Indeed, α-type ganglionar cells are much more transient than β-type ganglionar cells (see Figure 5), which is necessary for these cells to be efficient movement detectors. As a result, modeling a certain class of amacrine cells will be necessary when wishing to model α-type ganglionar cells.

Spatial non-linearity of α-type ganglionar cells. As explained in Section 2.2, α-type ganglionar cells do not respond linearly to the spatial structure of their input. More precisely, such cells are well modeled by a spatial pooling of rectified linear answers, as proposed by [21] amongst others. These linear answers are supposed to emerge from so-called linear 'sub-units'. Short-range amacrine cells certainly constitute a part of these so-called 'sub-units', along with bipolar cells [11].

Long-range synchronization of ganglionar cells. Studies led on correlation of spike trains from neighboring ganglionar cells [34, 5] have revealed that part of this synchronization might be imputable to amacrine cells, some of which make gap junctions with ganglionar cells (and thus have a very strong influence on their firing). [34] find strong correlations between the spike trains of ganglionar cells distant of several millimeters on the retina, a distance much bigger than the receptive fields of these cells. These synchronizations are probably due to long-range amacrine cells, that can be spiking cells with an axonic structure. However, the computational interest of such synchronization is unclear. Very interestingly, the synchronization only occurs when there is spatial continuity of the image between the two distant ganglionar cells, which could permit some low-level signaling of continuous objects, for example.

Dynamic adaptation to the visual scene. Synchronizations observed by [34] (previous paragraph) seemed to prove the influence of the particular visual scene on the firing of ganglionar cells, and not only through local calculations. In the same order of ideas, recent experiments [22] have shown that ganglionar cells dynamically adapt their receptive field to the recent geometrical properties of their environment. An intuitive explanation of this phenomenon is proposed, involving synaptic plasticity at the level of amacrine cells.

Other roles of amacrine cells. Particular classes of amacrine cells, like the AII rod amacrine cell, are directly linked to the *rod* visual pathway. AII amacrine cells are post-synaptic to rod bipolar cells, and make gap-junctions with *cone* ganglionar cells [31, 26]. Indeed, there are no rod-specific ganglionar cells in the retina and thus, AII amacrine cells play the role of transmitting the rod signal to ganglionar cells, which implies that our retinal output makes no physical distinction between the signals arising from cones or rods. Other amacrine cells are *dopaminergic*, and release this neurotransmitter directly into the inter-cellular space. Dopamine is released in the dark, and has physiological influences at different levels of the retinal pathway, to improve the SNR of visual processing in dark conditions. In particular, dopamine release augments the coupling of horizontal cells, and thus augments the spatial extent of the surround σ_S.

From this brief review of amacrine cells properties, their main role seems to be an *adaptive* shaping of ganglionar answers, as compared to the rather static architecture implemented by the retina in the OPL.

4.5 Assembling the Retina

The last step in modeling a retina is to assemble its elements with the specific radial structure of primate retinas. The fovea contains a high density of retinal cells and, subsequently, corresponds to small filtering scales σ_C and σ_S. Our retina is circular, with radius R_M. We assume that the mono-dimensional density for ganglionar cells, denoted by $d(r)$, is constant in the fovea (radius R_0) and then decreases in r^{-1} (log-polar density):

$$d(r) = \begin{cases} d_0 & \text{if } r < R_0, \\ d_0 R_0 / r & \text{if } r > R_0. \end{cases} \tag{40}$$

Conversely, the sizes of the spatial receptive fields, σ_C and σ_S, are constant in the fovea, and then augment proportionally to r. For example:

$$\sigma_C(r) = \begin{cases} \sigma_C^0 & \text{if } r < R_0, \\ \sigma_C^0 r / R_0 & \text{if } r > R_0. \end{cases} \tag{41}$$

This choice is based on the measurements of receptive fields for Parvocellular ganglionar cells in primate retinas [9], that vary proportionally to retinal eccentricity (see Section 2.3).

5 Results

This section presents quantitative results on modeled single cells and qualitative results on a whole array of cells. First, we fit the parameters of one model ganglionar cell with real responses of β-ganglionar cells. Second, we build a whole array of ganglionar cells to which we present images and moving sequences.

5.1 Experimental Protocol

Linear filtering (filter H_{Bip} in (36)) and spike generation (Section 4.4) were combined in a same object, representing one ganglionar cell. We then built an array of such objects, distributed along concentric circles and spaced inversely to $d(r)$ in (40). Gaussian noise was added in the positions to avoid aliasing.

Our ganglionar units use an *event-driven* spiking software, namely *Mvaspike* [39], that requires each neuron to be able to explicitly calculate the exact time of its next spike. More precisely, in an event-based software, every neuron recalculates the time of its next spike every time that its internal state is modified by external causes (such as pre-synaptic neurons). Then, all the new times of spikes are re-ordered, so as to find the next spike occurring in the network, etc. *Mvaspike* was originally created for recurrent networks without an external current [40]. But when modeling a retina, one has to integrate an *unknown* sensory input: the visual sequence, transformed into the input conductance $G^{exc}(t)$ on the ganglionar cell. So as for the neurons to be able to calculate exactly the times of their next spikes, through equation (2), the input $G^{exc}(t)$ to our ganglionar cells must be constant by parts. Subsequently, the potential of the ganglionar cells is exactly calculable: it is exponential by parts. Although a requirement of the event-based formalism, this method of integration can provide more efficient calculations that a step-by-step integration of (2), as we explain now.

In our model, the linear filtering in the OPL is calculated step-by-step, with a time step τ_{lin}. We thus calculate a *discrete* input to each ganglionar cell, $\{G^{exc}_{\Delta}(n)\}$, $n \in \mathbb{N}$. Then, one ganglionar cell performs *exact calculation* of the equation

$$\begin{cases} \frac{dV(t)}{dt} = G^{exc}_{\Delta}(t)(E^{exc} - V) - g^L V, \\ \\ \text{spike when } V(t) = 1, \text{ and absolute refractory period } \tau_R, \end{cases} \tag{42}$$

where $G^{exc}_{\Delta}(t) = G^{exc}_{\Delta}(n)$ for $t \in [n\tau_{\text{lin}}, (n+1)\tau_{\text{lin}}]$.

We insist that in our method, the calculation from $G^{exc}_{\Delta}(t)$ to the spike train of the ganglionar cell is exact, since the integration equation (42) is solvable exactly, $G^{exc}_{\Delta}(t)$ being constant by parts. In other words, the input $G^{exc}(t)$ to the ganglionar cell is approximated by $G^{exc}_{\Delta}(t)$, but not its subsequent spiking equation. This approach has two advantages, one theoretical and the other practical.

The theoretical advantage is a relatively clear understanding of the errors linked to discrete calculations. Let $\delta G(t)$ be the quantification error linked to our time discretization for linear calculations in the OPL, defined by $\delta G(t) = G^{exc}_{\Delta}(t) - G^{exc}(t)$. If no spikes

were produced by the ganglionar cell, the evolution of the cell's potential in response to $G^{exc}(t)$ would be given by equation (5). Then, let $\delta V(t)$ be the difference between respective responses to $G^{exc}_{\Delta}(t)$ and $G^{exc}(t)$. By basic integral inequalities starting from (5), one can link the maximum possible amplitude of $\delta V(t)$ as a function of the maximum amplitude in $\delta G(t)$. That is, if $\forall t, \delta G(t) < \epsilon$, then

$$\forall t, \delta V(t) < \left(\frac{E^{exc} + |E^{inh}|}{g^L} (1 + \frac{2G}{g^L}) \right) \epsilon,$$

where G is the maximum value for total conductance $g^{\infty}(t)$ in the cell. This allows us to control the precision required in the calculation of $G^{exc}_{\Delta}(t)$, as a function of the precision δV desired at the output of the cell (without spikes). Finally, if spikes are explicitly considered in the process, the preceding equation becomes false, but the quantification error δG can still be considered as a supplementary noise in the input conductance, and a noise whose law can be well approximated. Theory exists to link noise in the input to noise in the generated spike train [19, 6].

Apart from this theoretical advantage, our integration method has a practical interest. Indeed, the typical variations of the continuous input visual signal $G^{exc}(t)$ (given by $(1 + \alpha_C)\tau_C$ and $(1 + \alpha_S)\tau_S$ in our model, around 20 ms) are slower than the internal variations of the ganglionar cells' potential through (5), that are typically around 5 ms. Hence, the time step τ_{lin} needed to calculate the evolution of $G^{exc}_{\Delta}(t)$ can be about 5 times bigger than the time step that would be needed to implement the spiking equation (2) incrementally, meaning a computational gain.

However, using an event-based formalism is yet another issue than the simple integration method. In our present model, such formalism might seem a loss of time. What interest is there in finding, after each spike, the next spike that will occur at the level of the retina taken as a whole, if the ganglionar cells have no connections one to another? Worse, since all neurons integrate a continuous input, all internal states are necessarily modified at every step τ_{lin}, and as a result all neurons recalculate the time of their next spike, and all times for next spikes in the retina are reordered every τ_{lin}!

The interest is that our event-based formalism, although useless for the moment, allows all spike-based extensions of the model. One of the possible extensions is modeling spiking interactions between cells of the IPL, and how they can lead to specific synchronization effects [5, 34]. Another possible extension is to transform our retina model into a model for the Lateral Geniculate Nucleus (LGN), and model lateral spiking interactions, and even feedbacks from higher-level cortical areas: all the architecture for doing this is already present in our retina program.

From a computational point of view, the handicap of reordering all neurons every time step can be largely diminished, by reordering only those times of spikes that will occur in the next step of time τ_{lin}. Indeed, we know that the predicted time of spike for all other neurons are just estimations that are bound to be modified at the next time step. With this added procedure, useless calculations inherent to the event-based formalism are largely reduced, while all its advantages are kept.

5.2 Single Cell Simulations

We tested the response of single spiking cells to grating stimuli, by reproducing two series of measurements of [15] on cat X-cells. The length ratio between computer image and original cat retina was fixed so that one pixel corresponded to $0.1\,^\circ$ of arc. Thanks to this conversion we were able to fix the *center* and *surround* spatial extents σ_C and σ_S, based on the authors' measurements of the tested cell's receptive field. Temporal kernels for *center* and *surround* signals were arbitrarily fixed on biologically plausible values, with total delays respectively 20 ms and 60 ms. Non-linear synaptic transmission parameters were then chosen to fit the data. The experiments were repeated 30 times with noise added in the spike generation process as described in Section 4.4. Trial-averaged firing rates were then computed with a method similar to [15] (convolution of the spiking signal with a decreasing exponential kernel).

5.2.1 Drifting Gratings

In this experiment (Figure 14), moving gratings are presented to a cat X-ganglionar cell, with varying normal speeds and spatial frequencies. The spatial frequencies are respectively of 0.12, 0.26, 1.1 and 2 cycles per degree. Conversely, the speeds vary so that the temporal frequency remains constant, equal to 4 Hz.

In [15] the authors propose approximate values for σ_C and σ_S, for the X cell recorded in the experiment. Using the same values in our simulation, we find that simple linear filtering cannot reproduce the four cell responses of the original experience. Indeed, for frequency 1.1 cycles/degree (third line Figure 14), the modulation induced by the grating on the spatial answers of *center* and *surround* is more than ten times smaller than for frequencies 0.12 or 0.36 (first and second line Figure 14). If simple linearity was to be respected, this would imply modulations in the firing rate of the cell about ten times smaller in the case of frequency 1.1, which is obviously not the case. This is an experimental proof of the need for some non-linearity in retinal modeling. In our model, this role is played by the synapse from bipolar cells to the spiking ganglionar cell. Figure 15 represents the synaptic transmission function used in the experiment of Figure 14. The dashed lines represent the boundaries for the linear answer of the cell to the 1.1 stimulus, while the linear signal in the 0.36 experiment covers the whole abscissa. Thanks to synaptic non-linearity, the signal with small modulation is more amplified than the signal with big modulation. Note that further compression of the strong signals (0.12 and 0.36) appears in our model thanks to refractory period of the cells, set at 3 ms.

5.2.2 Static Grating

Another experiment (Figure 16) in [15] was to present a static grating to the tested cells, and suddenly reverse its contrast. The initial goal of the authors was to measure the spatial integration properties of these cells. Figure 16 compares results for their tested cell and our model. Qualitatively, our simulations are consistent with the measurements. However,

our model lacks the slow decrease that follows the sudden excitation of the cell. This slow decrease cannot be explained by a delayed *surround* signal. Indeed, the spatial extent σ_S, provided by the measures of [15], is too big for the *surround* component of the cell to be affected by the spatial phase of the grating. Whatever this phase, the cell's surround integrates enough stripes of the grating to always provide approximately the same signal.

Interestingly, this observation reveals the existence, in real retinas, of an additional temporal transiency, whose origin does not lie in the OPL. This is coherent with the findings of [7] in the Lateral Geniculate Nucleus (LGN). Experimental measures lead the authors to model LGN linear kernels with a filter similar to H_{Bip} (equation (36)), except for a supplementary transiency in the temporal parts of H_C and H_S. The reason why we have not introduced this additional transiency in our own model, is that its biological basis is unclear. Different possible origins are discussed in Section 6.

5.3 Simulation on an Array of Cells

This section presents realistic simulations for a channel of ON cells, with three kinds of stimuli: the apparition of a static image, the reaction to regular grids, and a sequence with a moving person on a static background. We represented our spiking output by adding, for each emitted spike, a circular spot on the image that holds with a latency of 50 ms. Temporally, this is equivalent to convolution of the spiking signal with a 50 ms step function, and provides a simplified simulation of synaptic integration in the LGN. Spatially, we varied the size of the spot and its intensity inversely with cell density at the eccentricity of the firing cell, so that the resulting image has the dimension of an instantaneous spiking frequency, independent of local cell density. The images shown here are displays normalized at each frame, for visibility. Animated videos of the simulations can be found at *http://www-sop.inria.fr/odyssee/team/Adrien.Wohrer/*.

5.3.1 Apparition of a Static Image

(Figure 17) We simulated the reaction of a retina to the sudden apparition of a static image. The cells were dark-adapted, meaning null signal for all cells before image onset, and the spiking process was without noise. The first spikes appear after 15 ms, and code the luminance signal (not contrast), because only the *center* signal has yet developed in the OPL. The brighter the zone, the faster the arrival of the first spike. In this experience, all cells fire their first spike before any cell fires its second, resulting in the uniform field for spike summation at 25 ms. This synchronous first wave is a consequence of our simplified simulation (no noise in spike generation, null initial condition for all cells). More realistic initial conditions in the experiment would lead to a destruction of this synchrony.

By contrast, in the second wave of spikes (time 31 ms), the cells situated on image edges (where *surround* signal is relatively weak) fire a little earlier, showing that the *surround* has already started to influence the cells on uniform zones. However, this time advance of edges in the second wave of spikes is very slight and depends a lot on the initial conditions. It takes more spikes for the signal to fully develop, independently of initial conditions. At

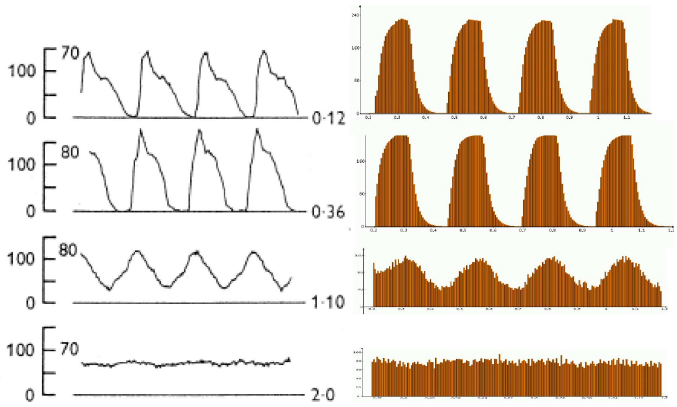

Figure 14: Trial-averaged firing rates of a real (*left column*, from [15]) and of a modeled (*right column*) ganglionar cell to drifting gratings with different spatial frequencies.

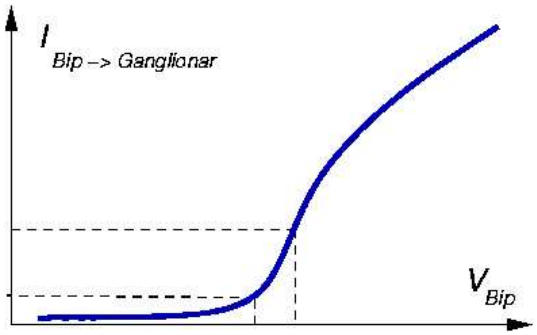

Figure 15: Static compression function linking bipolar linear answer to excitatory synaptic current in the ganglionar cell, for the drifting grating experience.

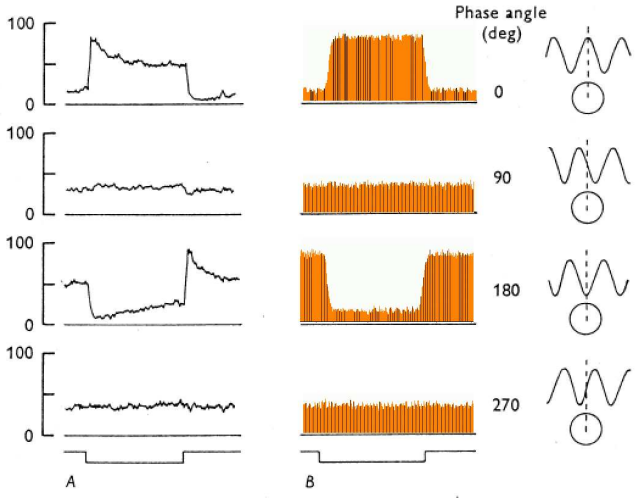

Figure 16: Trial-averaged firing rates of a real (*left column*, from [15]) and of a modeled (*right column*) ganglionar OFF cell to the reversal of a static grating, with different spatial phases.

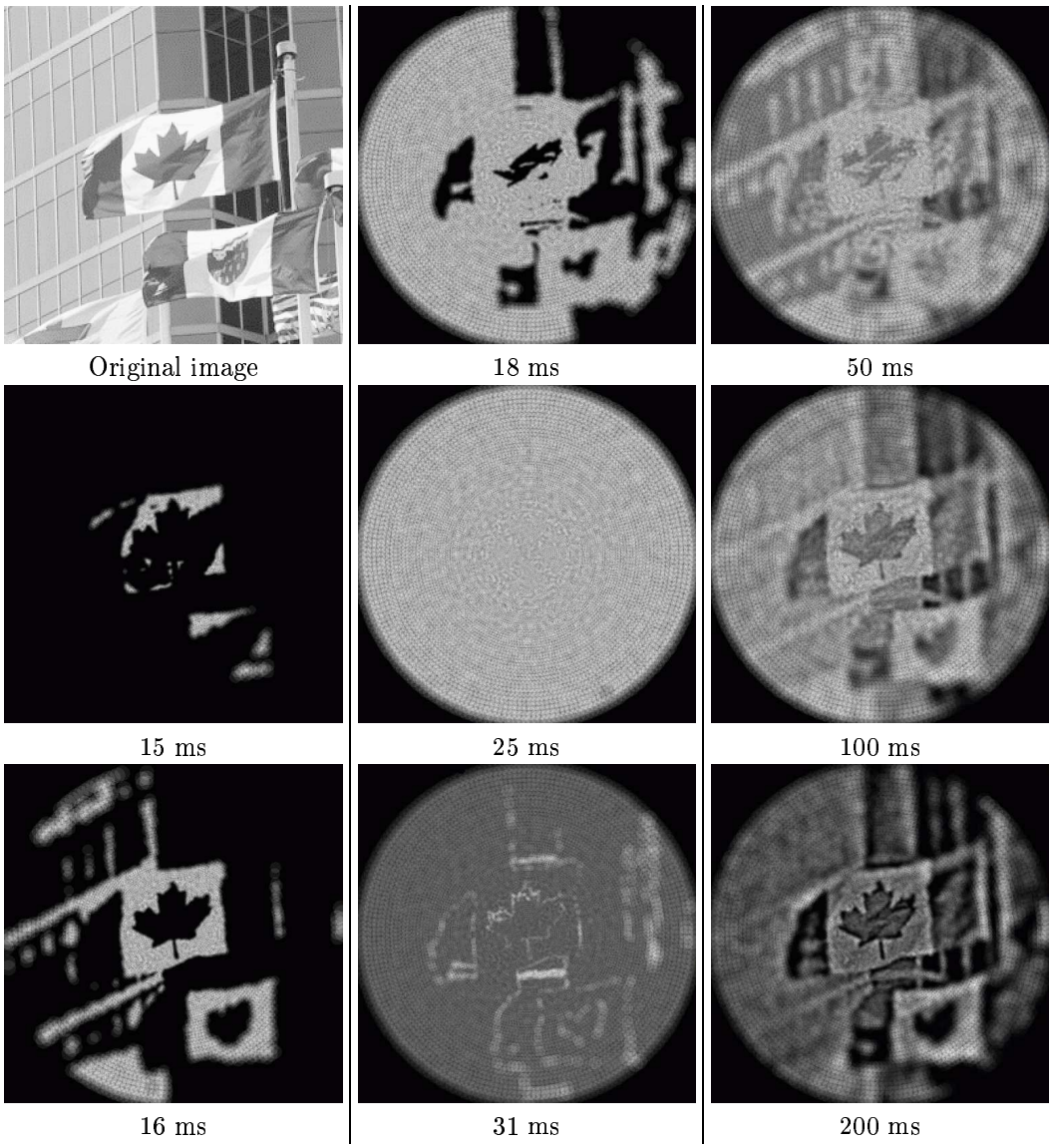

Figure 17: Response to a static image. *14440 units.* R_M *= 250 pix. Parameters in the fovea:* R_0 *= 50 pix,* d_0^2 *=0.66 cells/pix,* $\sigma_C = 1.5$ *pix and* $\sigma_S = 4.5$ *pix. For all cells,* $(\alpha_C + 1)\tau_C = 30$ *ms,* $(\alpha_S + 1)\tau_S = 60$ *ms,* $w = 0.9$. *Synaptic non-linearity was pure rectification.*

time 100 ms, the *center* component is still predominating, resulting in a reconstructed signal close to original image. One has to wait around 200 ms for the equilibrium regime to be reached, in which the *surround* has totally caught up with *center*. Then, the retina reacts to a mixture of spatial low-pass and band-pass properties, due to our choice of relative weight $w = 0.9$. This choice results in a predominance of edges, but with low firing in uniform zones as well. The foveation of the retina leads to less precise contours far from the center, seen for example in the rapid fading of the lines on the building.

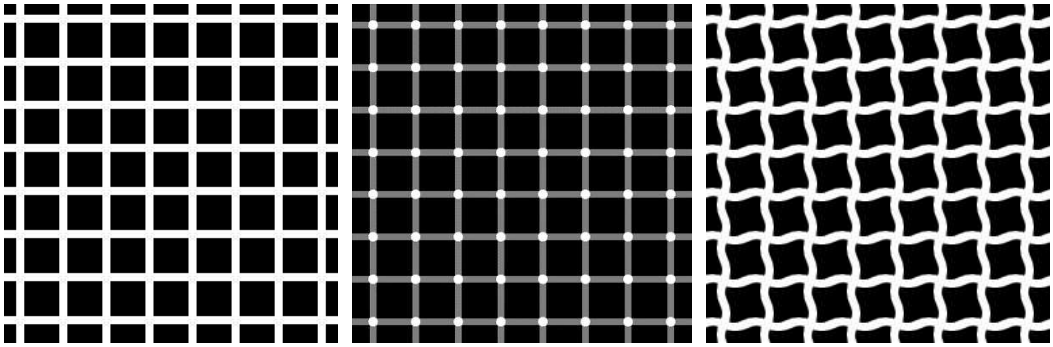

Hermann grid Scintillating grid Curved Hermann grid

Figure 18: Two grid stimuli inducing a perceptual illusion, and a counter-example Hermann grid (C) where the perceptual illusion is abolished.

5.3.2 Response to Grids

Particular visual illusions appear when moving eyes on regular grids. We tested the answer of an array of retinal cells to two grid stimuli. The first is the long-known Hermann grid (Figure 18 (A)), in which black spots appear at intersections of the grid. The second is the scintillating grid (Figure 18(B)) first proposed by [43], which is a Hermann grid with bright circles located at every intersection that appear to flicker when moving eyes on the grid.

The origin of these effects has long been thought to be retinal processing, since filtering by DOG filters of appropriate scales qualitatively reproduces the observed black spots at the center of the intersections. This simple view has recently been challenged by [18], through a new stimulus consisting of a Hermann grid with curved bars (Figure 18 (C)). If retinal processing was solely responsible for seeing the black spots, black spots would also be seen at intersection of this grid. They are not observed, meaning that the straight lines also have their importance in explaining the Hermann grid effect. However, it is possible that retinal processing play a role in the illusion, although seeing the illusion or not depends on higher-level interpretation of the retinal signal. We verified that, for appropriate parameters, the effect qualitatively observed in the Hermann grid and scintillating grid is reproduced by the output of our ganglionar cells.

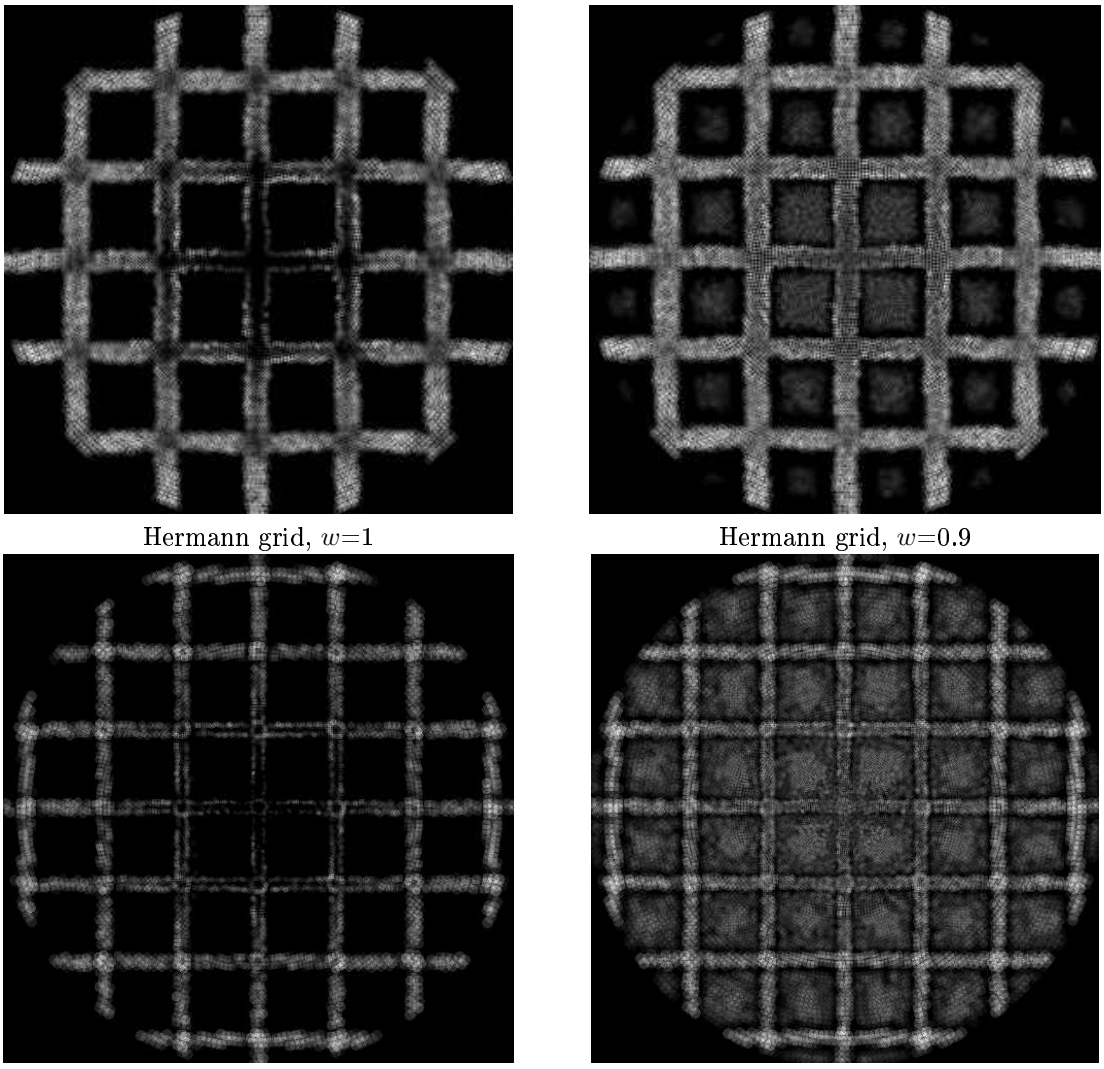

Hermann grid, w=1 Hermann grid, w=0.9

Scintillating grid, w=1 Scintillating grid, w=0.9

Figure 19: Response of the array of cells, 300 ms after image onset, to the two grid stimuli. Left column stimuli were made for totally transient filters ($w = 1$) whereas right column stimuli were made for partially transient filters ($w = 0.9$).

Figure 19 represents the answers of an array of ON ganglionar cells to a Hermann grid and a scintillating grid, with the similar reconstruction process as in preceding experiences, 300 ms after image onset. It qualitatively reproduces the perceived illusion, with less spikes at intersections. Parameters were fitted so as for the spatial scales σ_C and σ_S to augment a lot from center to periphery of the image, so as to display on these synthetic experiences all possible answers of the linear filter, according to its scale. The relative weight between *center* and *surround* was fixed, whether at 1, whether at 0.9. For $w = 1$, the filter acts as an edge detector. The further away from the fovea, the blurrier the edges, until the black spots at intersections totally disappear (at image periphery). On the contrary, in the fovea, edges are very sharp, and become almost invisible on the reconstructed image. For $w = 0.9$, the filter is also sensitive to the ground illumination of the images.

Although attractive, these results must be considered cautiously. First, of course, because the counter-example of Figure 18 (C) proves that the decreased spike firing at intersections acts only as an *indication* for visual perception, that can be enhanced or not by higher-level mechanisms such as detection of alignments. Second, there seems to be a difference of interpretation between the fovea and the periphery. Let us consider the case where $w = 1$ (left column of Figure 19). The visual illusion is interpreted as resulting from the decreased firing at the center of the spots. But the fovea, where the illusion is not perceived in real experiments, is in fact more silent than any other intersection in the image! Would this mean that the brain interprets differently a weak firing rate whether it is in the fovea or not? It is a possibility. Another possibility could be that weight w actually varies according to eccentricity. If w is smaller than one in the fovea, then the spike emission will rather resemble that of the right column of Figure 19, with a ground firing even in the uniform center of the intersection. Conversely, w could be closer to value one in the periphery, where detecting edges only reduces the total energy cost of transmission mediated by spikes. Such a hypothesis is plausible biologically, since the value of w is only linked to local synaptic weights, and its utility for retinal processing can be argued (see discussion in Section 6).

5.3.3 Moving Sequence

(Figure 20) We simulated the reaction of cells to a moving figure on a static background. The sequence was first presented to the cells at a normal pace (middle column), and then three times faster (right-hand side column), a pace for which the character becomes hard to follow accurately for a real human eye. Equivalently, our modeled cells performed well on the normal speed stimulus, but started losing spatial precision on the rapid stimulus, because the cell's linear filtering was not fast enough. It results in the blurry activation pattern over the character in the right-hand side column of Figure 20. The static background is also visible, with an accentuation on image edges (e.g. the texture of the bush in the background). This is expected when modeling β cells, which are known to provide input to the Form pathway of the brain. To have pure movement detectors such as α cells, a supplementary transient temporal filter would have to be added, to cut all signal on static objects. Such transiency is known to be provided on some ganglionar cells by a special class of amacrine cells [35].

Figure 20: Response to a moving sequence, at normal speed and accelerated speed (three times faster). *7308 units.* R_M *= 130 pix. Parameters in the fovea:* R_0 *= 40 pix,* d_0^2 *=0.66 cells/pix,* $\sigma_C = 1.5$ *pix and* $\sigma_S = 4.5$ *pix. For all cells,* $(\alpha_C + 1)\tau_C = 20$ *ms,* $(\alpha_S + 1)\tau_S = 60$ *ms,* $w = 0.9$. *Synaptic non-linearity was pure rectification.*

6 Discussion on the Present Model

The present model proposes an architecture for large scale simulations of an array of spiking β-type ganglionar cells. Our guideline was to stick as much as possible to biology, in the sense that every feature of the model can be related to a particular physiological location in the retina. By doing so, we built a platform for further experimentation, where we have good knowledge about which parts of retinal physiology are taken into account. Possible improvements starting from this retinal model are proposed in Section 7.

The main constraint we found to be imposed by retinal connectivity is the non-separability of filtering in the OPL. Because of its cellular implementation, the spatial *surround* signal is necessarily delayed temporally. When presented with a static image, this imposes that first spikes code only for the *center* signal, as displayed in Figure 17. As a result, spiking networks based on precise spike timings, e.g. those based on *rank coding* [17], cannot build precise models where the underlying linear filter is separable, consisting of a spatial difference of Gaussians modulated by a transient temporal filter. Spatial edges could, at best, be slightly coded by the *second wave* of spikes (Figure 17). The burst of activity at image onset due to the sole *center* signal could be more than just a drawback of retinal implementation, but rather an efficient transmission process. The initial phase could provide the whole visual information to the brain. Afterward, the residual retinal activity, prominent at image edges, associated to lateral interactions in the LGN and visual cortex such as *filling-in*, could be sufficient to maintain neural activity.

In our model, integration of *center* and *surround* signals at the level of bipolar cells implies a single weighting parameter w (Section 4.3) that concentrates the whole balance of a channel of units between low-pass and band-pass properties. To indeed display a visible mixture of both characteristics, we found the best weight w to be between 0.9 and 0.95. If smaller, the low-pass filter H_C, that has by construction a much larger gain than the band-pass difference $H_C - H_S$, becomes predominant. If bigger, the band-pass filter wins and no weak, ground signaling is displayed by the cells anymore. Such a value for w is close to the spatial ratio between *center* and *surround* measured in real X-cells [15].

The value of w is linked to the relative strengths of synapses from receptors and from horizontal cells at the level of bipolar cells (and also to the strength of the feedback from horizontal cells to bipolar cells, see Annex B). As a result, there is no evidence that this weight be a constant for different subtypes of bipolar cells, nor that it is a constant spatially. Our experiments on grids (Section 5.3.2) showed that a spatially inhomogeneous value for w could contribute to explain the particular reaction of the fovea to these stimuli. We suggested that w could be smaller in the fovea, leading to the absence of the scintillating effects at the very center of fixation. Although only a hypothesis, such proposition is not absurd. Filtering by a DOG in the retina is not necessary for higher-level tasks such as contour detection. Rather, it is a mean to limit the transmitted information to its most significant part (edges), and thus to limit calculations by the brain. The purpose of the fovea, precise analysis of the fixation point, might require that the foveal image be not limited to its edges, and thus lead to a relative weight w somewhat smaller than in the rest of the retina. Note that, through the CIF formalism in which both *center* and *surround* signals also appear as

divisive effects, this would not necessarily imply that the surround does not have effect on the firing of ganglionar cells in the fovea.

Our retinal model also demonstrates, through simulations on single cells such as that of Figure 14, the need for a non-linearity to reproduce the firing rates of real ganglionar cells. In its present state, the model explains this non-linearity by static, instantaneous synaptic compressions, and sums up the effects of these compressions in a unique non-linearity, modeling the synapse from bipolar cells to ganglionar cells.

We now come to the limitations of the present model. Some of its limitations, such as the simplified retinal connectivity (no feedback from horizontal cells to receptors, no amacrine cells), or modeling β-cells only, can be tackled in the same framework as that presented here, only by adding complexity to the connectivity in the model. Ameliorating the model in this way is feasible, and we discuss it in Section 7. Similarly, when building our retina model (Section 4), we have simplified our theoretical framework of CIF neurons (Section 3.1) to its linear range, that is to simple LIF neurons. This linear simplification appeared necessary to study retinal filtering, but some of the inherent non-linear effects in the CIF model can be grasped and included in the future model, as we explain in Section 7. However, some limits of the model also arise from the very theoretical framework we have chosen.

First, we have used point neurons. Real retinal cells have a spatial structure that could have some influence, especially in the retina where the cells' spatial display is directly responsible for the global filtering properties. Then, the CIF conductance model we use as a framework to all our calculations (Section 3.1), even considered with its possible non-linearities, does not grasp the diversity of ionic channels existing in a real retina, that have different Nernst potentials, different neurotransmitter release times, or even different working principles, since many receptors are not neurotransmitter-binding ionic channels[16]. Also, some voltage dependent channels exist even in the non-spiking retinal cells[17].

Another consequence of our simplified formalism is the loss of all intra-cellular adaptation phenomena, for example calcium adaptation that is supposed to play a crucial role in adaptation to light by cones [37, 42], with time constants of the order of one second [42]. Such intra-cellular adaptation effects could be present in all retinal cells, and provide explanations for the so-called cellular *fatigue*. In particular, cellular adaptation could provide another candidate for the slow decrease of the firing rate of ganglionar cells to a static input (Figure 16), since the time orders for the decrease in the firing rate is precisely that of calcium adaptation in cells. Although the concrete effects of adaptation are not hard to reproduce in our architecture (one just has to add a slow temporal transient at some point of retinal filtering), modeling its sources more precisely would require supplementary theoretical work that is not in the scope of our research for the moment.

What is the philosophy of the present simulator? We believe that one of its main interests is that it gives the possibility to implement large-scale arrays. This should help in confronting

[16] as in the *Cone–ON-bipolar* synaptic transmission, for example.

[17] As a matter of fact, cones *do* fire spikes when fed with a big current *in vitro*.

cell models, based on single-cell recordings, to their perceptual consequence at the level of an array of cells. We started such a study in Section 5.3, by simulating a whole array of ganglionar cells. In particular, the response to Hermann grids illustrates the possibility that such a model allows, to study large-scale answers to *optical illusions*. Indeed, optical illusions have always been a source of discoveries, and a benchmark for models, in visual neuroscience [13, 1]. We wish to use our retinal model to study some of the illusions whose origin lies in low-level visual processing. Similarly, we believe that the study of long-range retinal effects, such as long-range synchronization of the spikes from ganglionar cells (see Section 4.4.2) should somehow be confronted to its effects on large-scale simulations, rather than simply build appropriate mechanisms to reproduce cell-to-cell correlation diagrams. This could help in finding the behavioral advantage of such mechanisms.

However, all large-scale simulations require specific validation tools. For the moment, we have limited ourselves to linear convolutions starting from the spike train, and to visual appreciation of our results, which has us lose the interest of precisely modeling spike times. Research is currently developed in our lab to use the precise spike times emitted by our model retina for motion segmentation. Other validation tools for large-scale simulations, based on the precise times of spikes, should be thought of.

7 Future Work and Perspectives

As a last section to this report, we present possible future developments at this point of our work.

7.1 The CIF model and Contrast Gain Control

The CIF model presented as the framework to our calculations (Section 3.1) is very attractive in that its inherent non-linearities could explain non-linear effects experimentally observed in the retina. In Section 3.1.3 we separated two non-linear effects inherent to the CIF model. Both find echoes in published results about non-linear effects in the retina.

Varying time constants. The CIF formalism leads to an instantaneous filtering kernel at time t, $\xi \rightarrow K_t(\xi)$, that depends on the recent values of the total input conductance to the cell $g^\infty(t)$. As a result, when the inputs to the cells are big, all temporal scales in the retina should be shortened. Precisely, delays for retinal responses have been observed experimentally to depend of the contrast in the receptive field of the cell, with shorter delays for increasing contrast [48, 44] that is, for big answers of bipolar cells. This effect is known as *contrast gain control*. We believe that an explanation to this effect might come from the dynamically varying time constants of filtering induced by conductances in neurons, and modeled through our CIF formalism.

Divisive normalization. The second non-linearity of our CIF formalism is, in a non-spiking neuron, the scaling of the linear answer of the cell by its total conductance:

$$E^\infty(t) = \frac{G^{exc}(t)\,E^{exc} + G^{inh}(t)\,E^{inh} + I(t)}{G^{exc}(t) + G^{inh}(t) + g^L}. \tag{43}$$

At the level of bipolar cells, this would translate into a divisive effect between *center* and *surround* signals. And indeed, divisive effects between different linear filters have been used in recent retinal models [4], to explain non-linearities observed in retinal processing. Here also, we believe that a CIF formalism could provide such empirical models with a biological basis.

In which layers does conductance-based Contrast Gain Control appear? We believe that conductance-based effects can account for some observed non-linearities in retinal processing. However, it is not yet clear to us which layers of retinal processing are most concerned with this effect.

A natural candidate in the present state of the model would be bipolar cells, since they are the cells that first make a balance between *center* and *surround* signals, as opposite conductance openings $G^{exc}(t)$ and $G^{inh}(t)$ (or inversely for an OFF bipolar cell). However, applying the divisive normalization induced by (43) at the level of bipolar cells rather suggests an effect of invariance to luminosity, not to contrast. Indeed, if luminance should

be multiplied by two, it would cause $G^{exc}(t)$ (say, the *center* signal) and $G^{inh}(t)$ (say, the *surround* signal) to both be multiplied by two as well. But it would also make a bigger divisive term $G^{exc}(t) + G^{inh}(t) + g^L$, leading to an under-linear dependence of $E^{\infty}(t)$ with the scene luminance. This increased invariance to luminance, acting for 'small' variations of luminance (say, in less than a factor ten) would be complementary to the 'big' invariance to luminance provided by adaptation in photoreceptors (rather sensible to the logarithm of the luminance, as explained in Section 4.1.1).

Rather, filtering in the OPL results in a representation of contrast at the level of bipolar cells so, logically, *invariance* to contrast should rather be located in the IPL. This view is consistent with the findings of [30] that luminance gain control and contrast gain control are computational effects statistically independent in visual processing. However, equation (43) explains divisive scaling in *non-spiking cells* only (see Section 3.1.4) so, in the present state of our model, contrast gain control cannot be explained through the same divisive mechanism as that proposed for bipolar cells, that would be applied to ganglionar cells. Rather, we believe that conductance-induced normalizations in the IPL could be strong at the level of (non-spiking) amacrine cells, particularly through their reciprocal inhibitory conductances. Amacrine cells have long been thought to be one of the main sources of contrast adaptation in the retina.

7.2 Improving Retinal Connectivity

Our belief that some amacrine cells might be involved in Contrast Gain Control thanks to the conductance-based nature of their synapses, is a first necessity for our future work to model some classes of amacrine cells. This type of improvement consists in a refinement of the present connectivity in our model. Similar refinements could lead to two other developments.

Modeling α-type ganglionar cells. The model ganglionar cells presented in this report possess the underlying spatial linearity characteristic of mammalian β cells. Some additions should be made to model α-type ganglionar cells, e.g. cat Y cells or primate Parasol cells (Section 2.2). Several empirical models have been proposed to explain their filtering properties [21, 14], based on the findings that their receptive field arises from a pooling of the rectified linear answers of subunits in their receptive fields. However, uncertainty persists for the biological basis of these subunits. The most intuitive view, partly confirmed by the experimental findings of [11], is that these linear subunits are bipolar cells. Such an architecture is easily implementable in the framework proposed in this report. Indeed, our model for synaptic transmission (Section 3.2.4) includes a smooth rectification of the signal from bipolar cells. All that would be left to do is to provide our models α cells with synaptic inputs from a spatial pooling of bipolar cells, rather than from a single bipolar cell as in our present model (Section 4.4.1). However, the findings of [11] that bipolar pooling is not the only source of non-linearity in α cells, and also the additional transiency in the response of α cells (Section 2.2) would also necessitate to include at least one subtype of amacrine cells in the model.

Implementing long-range Synchronizations. Synchronizations between spikes from neighboring or distant ganglionar cells [5, 34] are though to be mediated by long-range amacrine cells, possibly through spikes (see Section 4.4.2). Although experimental findings still lack for this phenomenon, it could easily be studied with our retinal simulator. Indeed, its architecture is based on the spiking simulation software *Mvaspike* that is designed to model spiking interactions between neurons. Such a study, on a large scale simulator, could help understanding the possible advantages of such synchronizations in the retina.

7.3 Extension to a model of the LGN

Another possible use of the underlying spiking simulation software would be to directly implement a model of processing in the LGN. Indeed, spiking transmission from ganglionar cells to LGN cells is quite robust, in the sense that a spike in a ganglionar cell will reliably elicit a spike in its post-synaptic LGN cell. Experimental proofs of this fact can be found, for example, in the findings of [34] that the long-range correlations between ganglionar cells is also observed between cells of the LGN corresponding to the same retinotopic positions. As a result, one could consider our ganglionar units as being directly LGN cells and implement, through the spiking simulator, lateral interactions in the LGN, or even spiking feedbacks from a simplified model of the primary visual cortex.

Finally, our model could be extended to modeling of *two* retinas to work on binocular effects in the visual cortex. It can also include a preliminary image transformation to simulate rotation of the eyes and the resulting projection on a spherical surface.

8 Conclusion

We proposed a model for retinal processing based on the physiological structure of a retina. Its main filtering properties arise from the architecture of the OPL, where *center* and *surround* signals are created. Its first goal is to provide a spiking input to the brain, for higher-level, spike-based processing. As a result, our model includes the possibility of large-scale simulation, and can replicate the particular foveated structure of primate retinas. Furthermore, to allow experiments concerning precise spike timings, our model has a layer of spiking ganglionar cells, with biologically plausible noise sources.

The second goal is to provide a basis for further developments concerning the retina itself. Several aspects of retinal processing are not included yet, and will be the object of future work. For example we could extend the model to α-type ganglionar cells (*Magnocellular* pathway in primates) to provide an input to specific movement analysis modeling, or study synchronizations in the retina not explained by a simple linear filtering. Both these tasks require the modeling of certain categories of amacrine cells.

We also believe that special interest should be given to the conductance-based nature of membranar currents in retinal cells, that could provide such experimentally observed non-linear effects as Contrast Gain Control with a biological basis.

Acknowledgment

Thanks to O. Rochel for his spiking simulation software, and to the DyVa team and L. Perrinet in Marseille for fruitful exchanges. This work is realized within the scope of the European FACETS project.

A Convolution of Exponential Filters

In the retina, the transmission of visual signal through multiple layers of cell membranes and through chemical synapses induces a series of low-pass convolutions of the signal with decaying exponential filters. If linear, the related delays can be accounted for through a single filter, resulting from the convolution of many exponential filters, possibly with different characteristic times. This annex proposes a generic approximation for the resulting filter, depending on two time parameters $\tau_{\max}$ and τ_{dec}.

In this annex, we deal with normalized decaying exponential filters:

$$T_\tau(t) = \frac{1}{\tau} \exp\left(-\frac{t}{\tau}\right), \tag{44}$$

as that of Figure 21 (A), and try to calculate or approximate the filter resulting from a cascade of such exponential decays, whose convolution kernel is:

$$F_{\tau_1,\tau_2,\ldots,\tau_N}(t) = T_{\tau_1} * T_{\tau_2} * \cdots * T_{\tau_N} \ \ (t), \tag{45}$$

with some of the $\{\tau_n\}$ possibly being equal one to another.

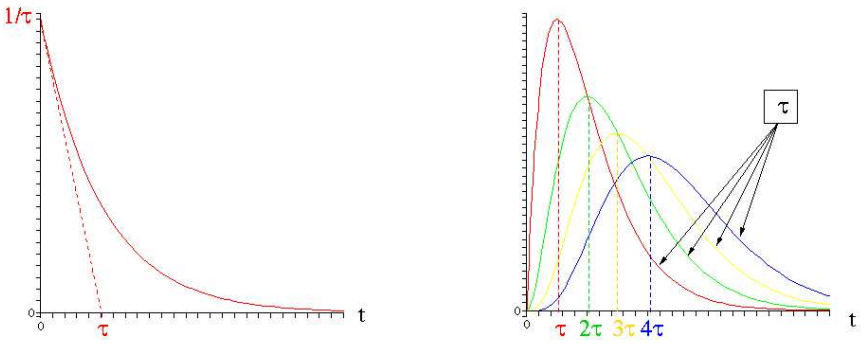

(A) Exponential kernel (B) Self-convolutions of an exponential kernel

Figure 21: An exponential kernel and its four first self-convolutions. All filters decay with the same characteristic time τ. Note that when n self-convolutions occur, the resulting filter peaks at time $n\tau$.

A.1 Exact Calculations

Self-convolution of a filter. From a few algebra, it appears that when one exponential filter is convolved with itself k times, the resulting filter is:

$$\underbrace{F_{\tau,\tau,\ldots,\tau}}_{k+1}(t) = T_{k,\tau}(t) = \frac{t^k}{\tau^{k+1}k!}\exp\left(-\frac{t}{\tau}\right). \tag{46}$$

This function is a positive 'blob' that reaches its maximum value at time $k\tau$ and then decays exponentially with a time constant τ (Figure 21 (B)). Note that (46) for $k = 0$ gives the filter in (44), meaning

$$T_{0,\tau} = T_\tau.$$

Convolution of different filters. Another derivable case is when exponential filters with different scales are convolved one to another. If N exponential filters T_{τ_n} are convolved, *with each τ_n being different from all the others*, the resulting filter writes:

$$\begin{aligned} F_{\tau_1,\tau_2,\ldots,\tau_N}(t) &= \sum_{n=1}^{N} \gamma_n\, T_{\tau_n}(t), \text{ with:} \\ \gamma_n &= \prod_{p\neq n} \frac{\tau_n}{\tau_n - \tau_p}. \end{aligned} \tag{47}$$

This function is also a positive 'blob' (Figure 22), but its peak time is not calculable anymore. Neither is its 'apparent' decay time, as defined by the strength of the decrease after the peak of the filter.

General case. Merging (46) and (47) should lead to a formula for the general case when N different exponential filters T_{τ_n} are convolved, with each filter n being cascaded K_n times. This most general case can be seen as a degenerated limit of (47) when different times get very close one to another. As a result, it also possesses the typical 'blobby' shape (Figure 22). It corresponds to a pondered sum of T_{k,τ_n} filters, with $k \in \{0, K_n\}$, but the corresponding coefficients $\gamma_{n,k}$ do not bear any simple expression anymore.

Calculating the transfer function. An alternative approach is to obtain the transfer function in the Fourier domain. This is straightforward, since convolution in the time domain corresponds to the multiplication in the Fourier domain. As a result, in the Fourier domain, any convolution of exponential filters has the following transfer function:

$$\widetilde{F}_{\tau_1,\tau_2,\ldots,\tau_N}(\xi) = \prod_{n=1}^{N} \frac{1}{1 - \mathbf{j}\tau_n\xi}, \tag{48}$$

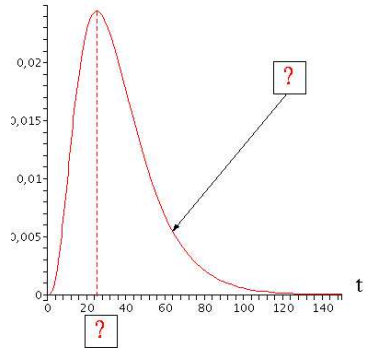

Figure 22: Convolution of exponential kernels with different decay times. Four filters were convolved here, with characteristic times of 5, 6, 10 and 15 ms, which are characteristic times for retinal low-pass filters (see report). Visually, the resulting filter still has typical rising time and decay time, but their exact calculation is impossible in general.

where some of the $\{\tau_n\}$ can possibly be equal one to another (general case).

Equation (48) is a more convenient way to work on the filter, since its properties are now described by a simple equation. Note also that coefficients γ_n in (47) can be obtained by reducing the total fraction of (48) in its simple elements. Similarly, one can derive the coefficients $\gamma_{n,k}$ for the general case, but the degenerated times τ_n lead to a term $1/(1-\mathbf{j}\tau_n\xi)^{K_n}$ in (48) that yields harder calculations for the simple elements' coefficients.

A.2 An Approximate Two-parameter Filter.

How can such an exponential cascade be described by few parameters? We believe that in the case of biological systems where all equations are approximate, a two-parameter model defined by a rising time $\tau_{\max}$ and a decay time τ_{dec} is a sufficient fit for any low-pass cascade.

The parametric function we use is defined by:

$$T_{\alpha,\tau}(t) = \frac{t^\alpha}{\tau^{\alpha+1}\Gamma(\alpha+1)} \exp\left(-\frac{t}{\tau}\right), \tag{49}$$

where α and τ are any real positive numbers. Γ is the mathematical Gamma function; it only serves as a normalization factor. Its most classical definition is precisely as being the integral of function $t^{\alpha-1}e^{-t}$ over $\mathbb{R}^+$, when $\alpha > 0$. Here again, notations are coherent. Indeed, function $x \to \Gamma(x+1)$ is an interpolation of the integer 'factorial' function. This means that (49) defines the same function as (46), when $\alpha \in \mathbb{N}$.

$T_{\alpha,\tau}$ is a function that reaches its maximum at time $\alpha\tau$, before decaying with time constant τ (Figure 23). Thus α and τ govern the two parameters we have chosen to describe our exponential 'blobs', with:

$$\begin{cases} \tau_{\max} = \alpha\tau, \\ \tau_{\text{dec}} = \tau. \end{cases} \tag{50}$$

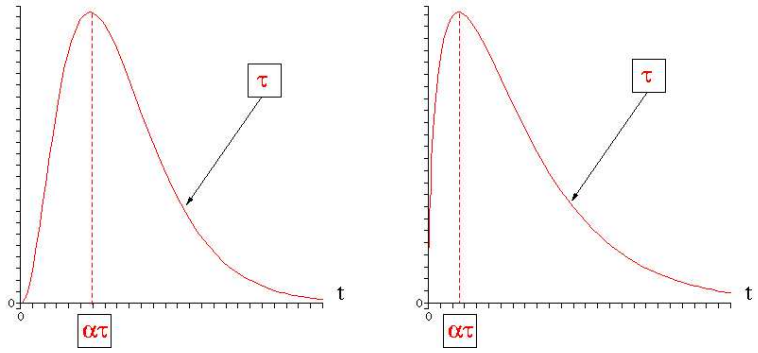

(A) $\alpha = 2.3$ (B) $\alpha = 0.5$

Figure 23: Two examples of kernel $T_{\alpha,\tau}$. Note that when $\alpha < 1$ (case (B)), the derivative of the kernel in $t = 0$ is always infinite. This is the main limitation for visual fitting of kernel $F_{\tau_1,\tau_2,\ldots,\tau_n}$ with a function $T_{\alpha,\tau}$ in some cases (see Figure 24).

Empirically one finds that any convolution of exponential filters is always well approached by some function $T_{\alpha,\tau}(t)$, except in its initial rising phase when the best fitting α is smaller than 1 (Figure 24). For this reason, we describe all retinal low-pass filters by appropriate functions $T_{\alpha,\tau}(t)$. However, one last question should be addressed. What links are there between the values for (α, τ) found empirically, and the times $(\tau_1, \tau_2, \ldots, \tau_n)$ of the original exponential filters that generated the blob?

Deriving parameters α and τ. We generated exponential cascades, numerically calculated the corresponding kernel, and looked for the visually best-fitting pair (α, τ). Empirically, we find out that for our best-fitting (α, τ), the sum of time-to-peak $\tau_{\max} = \alpha\tau$ and of decay time $\tau_{\text{dec}} = \tau$ is always close to the sum of all generating times. That is:

$$(1 + \alpha)\tau \simeq \sum_{n=1}^{N} \tau_n. \tag{51}$$

Empirically still, the visually best-fitting decay time τ for the whole cascade is a pondering of all individual exponential decay times, but with a pass filtersative contribution of big

(slow) exponential filters. That big time constants have a bigger impact on the decay time of the cascade is intuitive: a fast filter i in the cascade, with characteristic time $\tau_i \simeq 0$, does not modify the signal at all, so it cannot influence the visually best-fitting decay time. The simplest way to do this is to have each term in the sum pondered by its own value. And indeed, we find

$$\tau = \frac{\sum_{n=1}^{N} \tau_n^2}{\sum_{n=1}^{N} \tau_n} \tag{52}$$

to be a suitable choice for the decay time in most cases. Then, according to observation (51), we chose:

$$\alpha = \frac{\sum_{n=1}^{N} \tau_n}{\tau} - 1 \tag{53}$$

as our value for α. Using these approximations always provides a relatively correct fit of the real cascaded filter, as shown in Figure 24.

These empirical choices for (α, τ) can actually be justified in the Fourier domain. Indeed, one can check easily that the general Fourier transform of function $T_{\alpha,\tau}$ is given by:

$$\widetilde{T}_{\alpha,\tau}(\xi) = \frac{1}{(1 - \mathbf{j}\tau\xi)^{\alpha+1}}. \tag{54}$$

Then, developping the actual transfer function $\widetilde{F}_{\tau_1,\tau_2,\ldots,\tau_N}(\xi)$ of (48) and its approximation $\widetilde{T}_{\alpha,\tau}(\xi)$, both at the second order in ξ, provides:

$$\left\{ \begin{array}{l} \widetilde{F}_{\tau_1,\tau_2,\ldots,\tau_N}(\xi) = 1 + \mathbf{j}\left(\sum_{n=1}^{N} \tau_n\right)\xi - \frac{1}{2}\left((\sum_{n=1}^{N} \tau_n)^2 + \sum_{n=1}^{N} \tau_n^2\right)\xi^2 + o(\xi^2), \\ \text{and:} \\ \widetilde{T}_{\alpha,\tau}(\xi) = 1 + \mathbf{j}\left((\alpha+1)\tau\right)\xi - \frac{1}{2}\left(\tau^2(\alpha+1)(\alpha+2)\right)\xi^2 + o(\xi^2). \end{array} \right. \tag{55}$$

As a result, imposing that $\widetilde{T}_{\alpha,\tau}(\xi)$ be equal to $\widetilde{F}_{\tau_1,\tau_2,\ldots,\tau_N}(\xi)$ as far at the second order in ξ yields the approximation for α and τ that was empirically proposed in (52,53).

Best approximation with an integer α. Kernels $T_{\alpha,\tau}$ for which $\alpha \in \mathbb{N}$ have the computational advantage to be implementable through recursive filtering. Hence we also tested visual differences between the best-fitting $T_{\alpha,\tau}$ as described through (52,53) and its "integer alpha" approximation as defined by:

$$\left\{ \begin{array}{l} \alpha_{\mathbb{N}} = \text{round}(\alpha) \\ \tau_{\mathbb{N}} = \tau \dfrac{1+\alpha}{1+\alpha_{\mathbb{N}}}. \end{array} \right. \tag{56}$$

Function *round* returns the closest integer to α. $\tau_{\mathbb{N}}$ is still any real number, but it is calculated so as for $(\alpha_{\mathbb{N}}, \tau_{\mathbb{N}})$ to verify observation (51), or equivalently, to fit the first-order developments of Fourier transforms in (55) . This procedure still yields visually satisfying kernels, as illustrated in Figure 24.

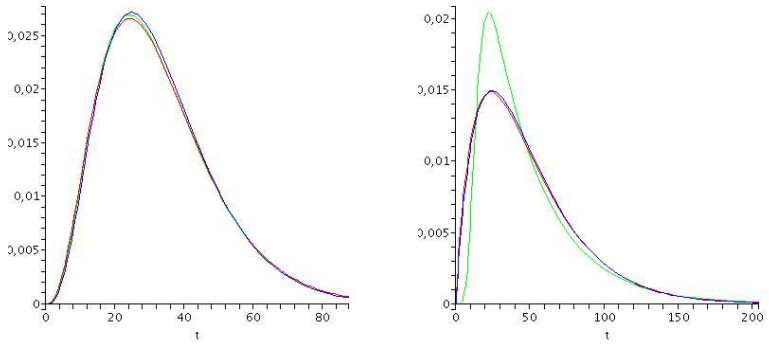

(A) $(8, 10^2, 15) \rightarrow (2.8, 11.5)$ (B) $(2^7, 35) \rightarrow (0.9, 25.5)$

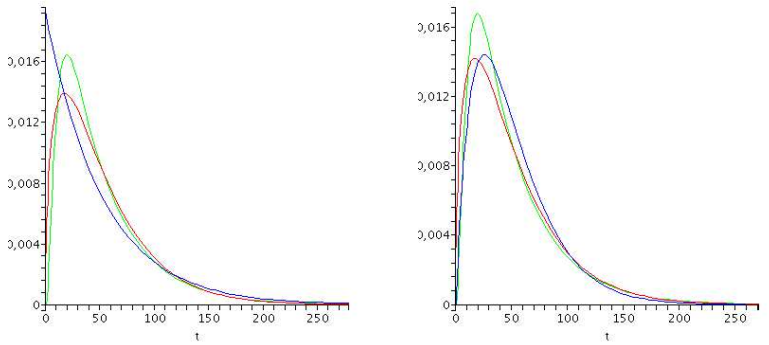

(C) $(5^2, 42) \rightarrow (0.49, 34.84)$ (D) $(5^2, 41) \rightarrow (0.50, 33.90)$

Figure 24: Four approximations of exponential cascades by $T_{\alpha,\tau}$ kernels. Notation is $(\tau_1, \tau_2, \ldots, \tau_N) \rightarrow (\alpha, \tau)$ using formulas (52,53). *Green Curve*: original cascade kernel. *Red Curve*: best approximation as described through (52,53). *Blue Curve*: Best approximation with integer α, as in (56). Figures comment: (A) very good fitting case. (B) problematic fitting case. The 7-fold repetition of exponential kernel $\tau = 2$ provides the real kernel with null derivatives in $t = 0$ at the 5 first orders, whereas the derivative of the approximate kernel is infinite, since $\alpha < 1$. (C) and (D) worst-case scenario for the fitting of best kernel $T_{\alpha,\tau}$ with an "integer α" kernel, through equation (56). A slight change of one of the original exponential times makes the best-fitting α cross value 0.5, yielding two different approximations for the Blue curve.

B Linear Modeling of the Feedback from Horizontal Cells

In this annex, we mention the possible effects of the feedback from horizontal cells to receptors, in a linear framework.

Horizontal Filter

Let $V_R(x,y,t)$ and $V_H(x,y,t)$ be the potentials of respectively receptor and horizontal layers. To allow exact calculations, we place ourselves in the linear framework, in which synapses are considered linear and instantaneous objects, and in which neurons are driven by currents, not conductances (meaning that we are in the linear simplification of the CIF model). The excitatory current on receptors provoked by phototransduction is noted $I^{exc}(x,y,t)$. Then, the feedback couples linearly $V_R(x,y,t)$ and $V_H(x,y,t)$, through two equations similar to (23):

$$\begin{cases} \dfrac{\mathrm{d}V_R}{\mathrm{d}t}(x,y,t) = \mathcal{G}_R\,\Delta V_R(x,y,t) - \tau_R^{-1}\,V_R(x,y,t) + I^{exc}(x,y,t) - (aV_H(x,y,t)+b) \\ \dfrac{\mathrm{d}V_H}{\mathrm{d}t}(x,y,t) = \mathcal{G}_H\,\Delta V_H(x,y,t) - \tau_H^{-1}\,V_H(x,y,t) + (cV_R(x,y,t)+d), \end{cases} \tag{57}$$

where $cV_R(x,y,t)+d$ represents the (linearized) excitatory current from receptors to horizontal cells, while $aV_H(x,y,t)+b$ represents the (linearized) feedback current from horizontal cells to receptors, which is always inhibitory.

Through subtraction of the static solution of this system, we can always suppose $b=0$ and $d=0$. Then, $V_H(x,y,t)$ and $V_R(x,y,t)$ bear Fourier transforms. In the Fourier space, (57) becomes

$$\begin{cases} -\mathbf{j}\xi_t\widetilde{V}_R(\xi_x,\xi_y,\xi_t) = \big(-\mathcal{G}_R(\xi_x^2+\xi_y^2) - \tau_R^{-1}\big)\widetilde{V}_R(\xi_x,\xi_y,\xi_t) + \widetilde{I}^{exc}(\xi_x,\xi_y,\xi_t) - a\widetilde{V}_H(\xi_x,\xi_y,\xi_t) \\ -\mathbf{j}\xi_t\widetilde{V}_H(\xi_x,\xi_y,\xi_t) = \big(-\mathcal{G}_H(\xi_x^2+\xi_y^2) - \tau_H^{-1}\big)\widetilde{V}_H(\xi_x,\xi_y,\xi_t) + c\widetilde{V}_R(\xi_x,\xi_y,\xi_t), \end{cases}$$

a system that can be explicitly solved, leading to the corresponding expression for transfer function for horizontal cells:

$$\widetilde{V}_H(\xi_x,\xi_y,\xi_t) = \widetilde{H}_H(\xi_x,\xi_y,\xi_t)\widetilde{I}^{exc}(\xi_x,\xi_y,\xi_t),$$

with

$$\widetilde{H}_H(\xi_x,\xi_y\xi_t) = \frac{c}{ac + \big(\tau_R^{-1} + \mathcal{G}_R(\xi_x^2+\xi_y^2) - \mathbf{j}\xi_t\big)\big(\tau_H^{-1} + \mathcal{G}_H(\xi_x^2+\xi_y^2) - \mathbf{j}\xi_t\big)}. \tag{58}$$

This is also the asymptotical expression found by J. Herault in the case of a discrete array of cells, in his (yet unpublished) book about the retina.

The influence of the feedback can be directly measured through (58), that involves the total gain of the feedback loop, ac. By studying the derivatives of $\widetilde{H}_H(\xi_x,\xi_y,\xi_t)$ with respect

to ξ_x, ξ_y and ξ_t, one can tell whether the horizontal filter is low-pass or band-pass. After calculations, it appears that the horizontal filter defined by $\widetilde{H}_H$ is always low-pass spatially, in the sense that

$$\forall(\xi_x,\xi_y,\xi_t),\quad \frac{\partial\|\widetilde{H}_H\|}{\partial|\xi_i|}(\xi_x,\xi_y,\xi_t)<0,$$

for $i=x,y$.

On the contrary, the horizontal filter can become band-pass *temporally*, if the gain of the feedback loop becomes big enough. More precisely, at a given spatial frequency (ξ_x,ξ_y), the function

$$\xi_t \rightarrow \|\widetilde{H}_H\|(\xi_x,\xi_y,\xi_t)$$

reaches its maximum at temporal frequency

$$|\xi_t| = \sqrt{ac - \frac{\left(\tau_R^{-1}+\mathcal{G}_R(\xi_x^2+\xi_y^2)\right)^2+\left(\tau_H^{-1}+\mathcal{G}_H(\xi_x^2+\xi_y^2)\right)^2}{2}}, \tag{59}$$

provided the feedback ac is big enough for the term inside the square root to be positive. This means that, theoretically, temporal resonances can appear in the responses of horizontal cells to a time-varying stimulation, with peak of resonance dependent on the spatial spectrum of the stimulus.

Receptor Filter

In turn, the potential of horizontal cells $V_H(x,y,t)$ is fed back to receptors, through the first equation of (57). As a result, temporal resonances, if they exist, will also be observed at the level of the receptor's potential $V_R(x,y,t)$. Small oscillations are indeed observed by [42] in the impulse response of some cones to brief flashes of light, as depicted in Figure 25. The authors attribute these oscillations to the nature of the phototransduction process (that also involves feedback loops), that would provide by itself the biphasic shape of the cones' linear answer (see Section 4.1.2). Given their experimental protocol, we claim that the biphasic shape and the oscillations more likely correspond to the feedback from horizontal cells, and involve other conductances than phototransduction itself.

Bipolar Filter

In primate retinas, horizontal cells display both feedback connections to receptors, and feed-forward connections to bipolar cells [26]. As a result, the bipolar filter is still calculated as a pondered sum of the signals from receptors and horizontal cells, as in Section 4.3. The bipolar filter can still be written

$$H_{\mathrm{Bip}} = H_C - wH_S, \tag{60}$$

where H_C corresponds to the direct transmission from receptors, and H_S corresponds to the part of the signal that has transited through horizontal cells. However, H_S is now composed

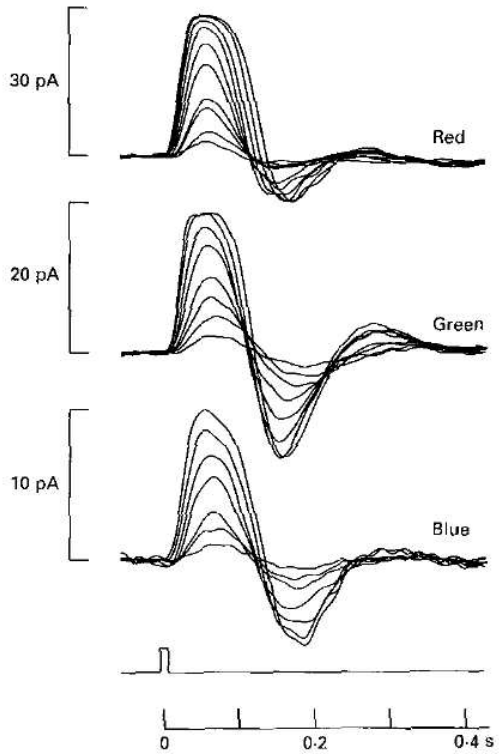

Figure 25: Current flowing through three cones, one of each type, that have been dark adapted, in response to flashes of light. The linear answer is always biphasic, and can even display attenuated oscillations (here, for the 'Green' cone). From [42].

of two terms:

$$H_S = H_S^{FF} + H_S^{FB}.$$

H_S^{FF} corresponds to the part of the bipolar signal resulting from feed-forward transmission from horizontal to bipolar cells, while H_S^{FB} corresponds to the part of the signal that transits again by receptors, through the feedback from horizontal cells. Due to the possible band-pass properties of horizontal filter H_H (equation (58)), H_C, H_S^{FF} and H_S^{FB} can all display a slight oscillatory response, but the recordings of Figure 25 as well as experimental recordings on bipolar cells insure that this effect, if present, is weak. Furthermore, H_S^{FB} corresponds to a signal that transits through one more layer of cells (receptors, after horizontal cells), and thus is a bit more low-passing than H_S^{FF} the direct signal from horizontal cells. But coupling of horizontal cells is still the main contribution to the spatial extent of both filters H_S^{FF} and H_S^{FB}. For this reason, the expression proposed in Section (4.3)

$$\begin{cases} H_C(x,y,t) = G_{\sigma_C}(x,y) T_{\alpha_C,\tau_C}(t), \\ \\ H_S(x,y,t) = G_{\sigma_S}(x,y) T_{\alpha_S,\tau_S}(t). \end{cases}$$

still appears a reasonable approximation for the bipolar filter, even when considering feed-back from horizontal cells to receptors.

References

[1] M. Bach. Optical illusions and Visual phenomena. Web : http://www.michaelbach.de/ot/index.html, 2006.

[2] H.B. Barlow and W. R. Levick. The mechanism of directionally selective units in rabbit's retina. *J Physiol*, 178:477–504, 1965.

[3] D. A. Baylor, T. D. Lamb, and K. W. Yau. The membrane current of single rod outer segments. *Journal of Physiology*, 288(1):589–611, 1979.

[4] V. Bonin, V. Mante, and M. Carandini. The suppressive field of neurons in Lateral Geniculate Nucleus. *Journal of Neuroscience*, 25(47):10844–10856, November 2005.

[5] I. H. Brivanlou, D. K. Warland, and M. Meister. Mechanisms of concerted firing among retinal ganglion cells. *Neuron*, 20:527–529, March 1998.

[6] Nicolas Brunel, Frances S. Chance, Nicolas Fourcaud, and L. F. Abbott. Effects of synaptic noise and filtering on the frequency response of spiking neurons. *Physical Review Letters*, 86(10), 2001.

[7] D. Cai, G. C. Deangelis, and D. Freeman. Spatiotemporal receptive field organization in the lateral geniculate nucleus of cats and kittens. *Journal of Neurophysiology*, 78(2):1045–1061, August 1997.

[8] D. Colella. Web : http://www.mitre.org/news/the_edge/september_99/fifth.html, 1999.

[9] D. Dacey and M. Peterson. Dendritic field size and morphology of midget and parasol ganglion cells of the human retina. *Proc Natl Acad Sci*, 89:9666–70, 1992.

[10] P. Dayan and L. F. Abbott. *Theoretical Neuroscience : Computational and Mathematical Modeling of Neural Systems*. MIT Press, 2001.

[11] J. B. Demb, K. Zaghloul, L. Haarsma, and P. Sterling. Bipolar cells contribute to nonlinear spatial summation in the brisk-transient (Y) ganglion cell in mammalian retina. *Journal of Neuroscience*, 21(19):7447–7454, October 2001.

[12] A. Destexhe, M. Rudolph, and D. Paré. The high-conductance state of neocortical neurons in vivo. *Nature Reviews Neuroscience*, 4:739–751, 2003.

[13] D. M. Eagleman. Visual illusions and neurobiology. *Nature Reviews Neuroscience*, 2:920–926, 2001.

[14] C. Enroth-Cugell and A. W. Freeman. The receptive-field spatial structure of cat retinal Y cells. *Journal of Physiology*, 384(1):49–79, 1987.

[15] C. Enroth-Cugell and J. G. Robson. The contrast sensitivity of retinal ganglion cells of the cat. *J Physiol*, 187:517–552, 1966.

[16] T. Euler and R. H. Masland. Light-evoked responses of bipolar cells in a mammalian retina. *J. Neurpohysiology*, 83(4):1817–1829, April 2000.

[17] J. Gautrais and S. Thorpe. Rate coding vs temporal order coding : a theorical approach. *Biosystems*, 48:57–65, 1998.

[18] J. Geier, L. Sera, and L. Bernath. Stopping the hermann grid illusion by simple sine distortion. In *ECVP*, 2004.

[19] W. Gerstner and W. Kistler. *Spiking Neuron Models.* Cambridge University Press, 2002.

[20] J. Herault. A model of colour processing in the retina of vertebrates: from photoreceptors to colour opposition and colour constancy phenomena. *Neurocomputing*, 12:113–129, 1996.

[21] S. Hochstein and R. M. Shapley. Linear and nonlinear spatial subunits in Y cat retinal ganglion cells. *J Physiol*, 262:265–284, 1976.

[22] T. Hosoya, S. A. Baccus, and M. Meister. Dynamic predictive coding by the retina. *Nature*, 436:71–77, 2005.

[23] D. H. Hubel and T. N. Wiesel. Receptive fields of optic nerve fibres in the spider monkey. *J. Physiol.*, 154:572–80, December 1960.

[24] J. Keat, P. Reinagel, R. C. Reid, and M. Meister. Predicting every spike: a model for the responses of visual neurons. *Neuron*, 30:803–817, 2001.

[25] H. Kolb. The inner plexiform layer in the retina of the cat: electron microscope observation. *Journal of Neurocytology*, 8:295–329, 1979.

[26] H. Kolb, E. Fernandez, and R. Nelson. Webvision : the Organization of the Retina and Visual System. Web : http://webvision.med.utah.edu/, 2001.

[27] T. W. Kraft, D. M. Schneeweis, and J. L. Schnapf. Visual transduction in human rod photoreceptors. *Journal of Physiology*, 464(1):747–765, 1993.

[28] T. D. Lamb. Spatial properties of horizontal cell responses in the turtle retina. *J Physiol*, 263(2):239–55, 1976.

[29] M. A. Mahowald and C. Mead. The silicon retina. *Sci. Am.*, 264(5):76–82, 1991.

[30] V. Mante, R. A. Frazor, V. Bonin, W. S. Geisler, and M. Carandini. Independence of luminance and contrast in natural scenes and in the early visual system. *Nature Neuroscience*, 2005.

[31] R. Masland. The fundamental plan of the retina. *Nature neuroscience*, 4(9), September 2001.

[32] D. Weedman Molavi, J. Price, H. Burton, and D. Van Essen. The W.U.S.M Neuroscience Tutorial. Web : http://thalamus.wustl.edu/course/, 1997.

[33] K. I. Naka and W. A. Rushton. The generation and spread of s-potentials in fish (cyprinidae). *J Physiol*, 192(2):437–61, September 1967.

[34] S. Neuenschwander and W. Singer. Long-range synchronization of oscillatory light responses in the cat retina and lateral geniculate nucleus. *Nature*, 379(6567):728–732, February 1996.

[35] S. Nirenberg and M. Meister. The light response of retinal ganglion cells is truncated by a displaced amacrine circuit. *Neuron*, 18:637–650, 1997.

[36] G. Osterberg. Topography of the layer of rods and cones in the human retina. *Acta Ophthal.*, suppl. 6:1–103, 1935.

[37] A. Polans, W. Baehr, and K. Palczewski. Turned on by Ca^{2+}! The physiology and pathology of Ca^{2+}-binding proteins in the retina. *Trends in Neurosciences*, 19(12):547–554, December 1996.

[38] F. Rieke and D. A. Baylor. Single-photon detection by rod cells of the retina. *Rev. Mod. Phys.*, 70(3):1027–1036, July 1998.

[39] O. Rochel. *Une approche événementielle pour la modélisation et la simulation de neurones impulsionnels.* PhD thesis, Université Henri Poincaré - Nancy 1, 2004.

[40] O. Rochel and D. Martinez. An event-driven framework for the simulation of networks of spiking neurons. In *Proc. 11th European Symposium on Artificial Neural Networks*, pages 295–300, 2003.

[41] R.W. Rodieck. Quantitative analysis of cat retinal ganglion cell response to visual stimuli. *Vision Research*, 5:583–601, 1965.

[42] J. L. Schnapf, B. J. Nunn, M. Meister, and D. A. Baylor. Visual transduction in cones of the monkey macaca fascicularis. *J Physiol*, 427(1):681–713, 1990.

[43] M. Schrauf, B. Lingelbach, and E. R. Wist. The scintillating grid illusion. *Vision Research*, 37(8):1033–1038, 1997.

[44] R. Shapley and J. D. Victor. The contrast gain control of the cat retina. *Vision Res.*, 19(4):431–434, 1979.

[45] R. M. Shapley and J. D. Victor. The effect of contrast on the transfer properties of cat retinal ganglion cells. *The Journal of Physiology*, 285(1):275–298, 1978.

[46] L. Tao, M. Shelley, D. McLaughlin, and R. Shapley. An egalitarian network model for the emergence of simple and complex cells in visual cortex. *Proc Natl Acad Sci*, 101(1):366–371, January 2004.

[47] J.M. Valeton and D. Van Norren. Light adaptation of primate cones : An analysis based on extracellular data. *Vision Research*, 23(12):1539–1547, 1983.

[48] J. D. Victor. The dynamics of the cat retinal X cell centre. *The Journal of Physiology*, 386(1):219–246, 1987.

[49] J. D. Victor. Temporal aspects of neural coding in the retina and lateral geniculate. *Network: Computation in Neural Systems*, 10(4):R1–R66, November 1999.

[50] D. J. Wielaard, M. Shelley, D. McLaughlin, and R. Shapley. How simple cells are made in a nonlinear network model of the visual cortex. *The Journal of Neuroscience*, 21(14):5203–5211, July 2001.

Unité de recherche INRIA Sophia Antipolis
2004, route des Lucioles - BP 93 - 06902 Sophia Antipolis Cedex (France)

Unité de recherche INRIA Futurs : Parc Club Orsay Université - ZAC des Vignes
4, rue Jacques Monod - 91893 ORSAY Cedex (France)
Unité de recherche INRIA Lorraine : LORIA, Technopôle de Nancy-Brabois - Campus scientifique
615, rue du Jardin Botanique - BP 101 - 54602 Villers-lès-Nancy Cedex (France)
Unité de recherche INRIA Rennes : IRISA, Campus universitaire de Beaulieu - 35042 Rennes Cedex (France)
Unité de recherche INRIA Rhône-Alpes : 655, avenue de l'Europe - 38334 Montbonnot Saint-Ismier (France)
Unité de recherche INRIA Rocquencourt : Domaine de Voluceau - Rocquencourt - BP 105 - 78153 Le Chesnay Cedex (France)

Éditeur
INRIA - Domaine de Voluceau - Rocquencourt, BP 105 - 78153 Le Chesnay Cedex (France)
http://www.inria.fr
ISSN 0249-6399